Chapter 2
A Review of Positive Electrode Materials for Lithium-Ion Batteries

Masaki Yoshio and Hideyuki Noguchi

2.1 Recent Cathode Materials

The lithium-ion battery generates a voltage of more than 3.5 V by a combination of a cathode material and carbonaceous anode material, in which the lithium ion reversibly inserts and extracts. Such electrochemical reaction proceeds at a potential of 4 V vs. Li/Li^+ electrode for cathode and ca. 0 V for anode. Since the energy of a battery depends on the product of its voltage and its capacity, a battery with a higher energy density is obtained for a material with a higher voltage and a higher capacity. Therefore, when the same anode material is used, the higher the cathode potential and the larger the capacity of the cathode material, the higher the energy of the battery.

The cathode and anode were packed into a vessel with constant dimensions, so the capacity for unit volume is more important than for weight. The volumetric-specific capacity of $LiCoO_2$ is 808 mAh/cm^3, which is high enough to be used as a cathode material. Nickel-based cathode materials deliver higher capacity of 870–970 mAh/cm^3. Safety problems for this material are overcome by the simultaneous doping of cobalt and aluminum. SAFT Co. has adopted $LiNi_{0.8}Co_{0.15}Al_{0.05}O_2$ supplied by Toda Kogyo Co. (formerly Fuji Chemical Industry Co.) as a cathode material in the lithium-ion battery for an electric vehicle (EV) application. An analogous compound is used in Japan. A press release announced that the capacity of it is 20% higher than that of $LiCoO_2$ and it is safer than $LiCoO_2$ in terms of overcharge problems. Further, nickel-based cathode materials are used for the battery in Toyota's car, without idling.

Manganese spinel cathode materials, although inferior to layered compounds, are cheap and rich in resources. Therefore, it is suitable as a cathode material in large-scale use of lithium-ion batteries. This spinel compound has been used for cellular phones produced by NEC Co. and for EV and hybrid EV produced by Nissan Co. Ltd. However, its share in the market of cathode material is relatively

M. Yoshio (✉) and H. Noguchi
Department of Applied Chemistry, Saga University, Saga 840-8502, Japan
yoshio@cc.saga-u.ac.jp
GBE03502@nifty.com

M. Yoshio et al. (eds.), *Lithium-log Batteries*,
DOI 10/1007/978-0-387-34445-4_2

small. Recently, in 2003, electric mortar bicycles and mortar-assisted bicycles have been commercialized. In such applications, the cathode contains manganese spinel compounds. This trend would lead to the development in large-scale use of batteries using a spinel compound as a cathode material.

The main cathode material, $LiCoO_2$, in the lithium-ion battery has been improved in terms of rate capability and capacity. The rate capability is improved by the control of particle morphology, and high capacity is achieved by increased charge voltage while overcoming safety problem.[1]

2.2 The Structure of Cathode Material

Many of the lithium battery cathode materials have a layered structure, which enables the two-dimensional diffusion of the lithium ion, or a spinel structure, which enables the three-dimensional diffusion. The structures of the cathode materials in the lithium- ion battery are summarized, together with its electrochemical properties and stability of structure, in Table 2.1.

The basic compounds with a layered structure are $LiCoO_2$, $LiNiO_2$, $LiCrO_2$, Li_2MoO_3, and $Li_{0.7}MnO_2$. The initial three compounds have a rhombohedral structure with the symmetry of space group $R\bar{3}_m$. As shown in Fig. 2.1, the rhombohedral unit cell has a geometric feature that has three axes of an equal length, and that each angle between any two axes is the same. Usually, this unit cell is expressed by the hexagonal structure (heavy line in the figure), which has a unit cell volume of three times because the structure of this unit cell is difficult to be imaged. In this structure, Li and transition metal ion (M) occupy alternatively an octahedral site formed by planar O^{2-} ion sheet; as a result, the Li layer and M layer are formed.

The structure of Li_2MnO_3 is slightly deviated from above one, namely, the M ion is replaced by $Li_{1/3}Mn_{2/3}$. Electroactive materials with this structure are Li_2RuO_3, Li_2IrO_3, Li_2PtO_3, and $Li_{1.8}Ru_{0.6}Fe_{0.6}O_3$. These compounds contain an expensive noble metal, so they are unsuitable for practical application. There are many layered electroactive materials prepared by foreign metal ion and lithium doping. These compounds would be classified into two groups. One is a substitution product and the other is the solid solution-type compound. The differences of the two compounds are explained in the $LiNiO_2$–$LiMnO_2$–Li_2MnO_3 quasiternary phase diagram (Fig. 2.2). Three corners in triangles indicate pure phases. The middle point of the $LiNiO_2$–$LiMnO_2$ line has a composition of $LiNi_{1/2}Mn_{1/2}O_2$, where valences of Ni and Mn are estimated to be 2^+ and 4^+, respectively, by the analysis of the XANES spectra of the K edge absorption of Ni and Mn.[2] Therefore, the substitution reaction of Ni^{3+} by $1/2Ni^{2+} + 1/2Mn^{4+}$ proceeds on the line and all the Ni^{3+} ion is consumed at the middle point. A series of single-phase products are easily prepared for the compositions on the $LiNiO_2$–Li_2MnO_3 and $LiNi_{1/2}Mn_{1/2}O_2$–Li_2MnO_3. These products are generally called a "solid solution," in which valences of metal ion are equivalent to those of two end members in all the composition range. Therefore, the shadow areas are solid solutions between Li_2MnO_3 and $LiNi_xMn_{1-x}O_2$ ($x \geq 0.5$).

Table 2.1 Properties of anode and cathode materials for lithium ion battery

Cathode							
Material	Pr. Cap. (mAh/g)	Density (g/cc)	Vol. En. Den. (mAh/cc)	Shape of Dis. curve	Safety	Cost	Comment
$LiCoO_2$	160	5.05	808	Flat	Fair	High	Small-size
$LiNiO_2$	220	4.80	1,056	Sloping	Poor	Fair	Impossible
$LiNi_{0.8}Co_{0.2}0_2$	180	4.85	873	Sloping	Fair	Fair	LIP? Small scale
$LiNi_{0.8}Co_{0.15}Al_{0.05}O_2$	200	4.8	960	Sloping	Fair	Fair	LIP? Small scale
$LiMn_{0.5}Ni_{0.5}O_2$	160	4.70	752	Sloping	Good	Low	?
$Li\ Mn_{1/3}\ Ni_{1/3}Co_{1/3}O_2$	200	4.7		Sloping	Good	Low	
$Li\ Mn_{0.4}Ni_{0.4}Co_{0.2}O_2$	200	4.7					
$LiMn_2O_4$	110	4.20	462	Flat	Good	Low	HEV, EV
$Li_{1.06}Mg_{0.06}Mn_{1.88}O_4$	100	4.20	420	Flat	Good	Low	HEV, EV
$LiAlMnO_4$							
$LiFePO_4$	160	3.70	592	Flat	Good	Low	Low cond.

Carbon anode	Crystallinity[a] (%)	Practical capacity (mAh/g)	Comment
Spherical graphatized mesocarbon microbeads (MCMB)	82.7	320–330	Easy coating
Graphatized carbon fiber (MCF)	89.7	320–330	Stopped to produce
Pitch base graphite	91.6–94.4	~350	Largest share in the market with electrolyte additives
Carbon-coated natural graphite	100	360 ~ 365	Less decomposition of electrolyte without additives

Alloy anode	Discharge voltage (V vs. Li/Li^+)	Capacity (mAh/g)	Density (g/cm^3)	Capacity/volume (mAh/cm^3)	Comment maximum swelling (MS)
Li	~0	1,840	0.5	1,920	Safety
Sn	0.65	990	7.3	7,230	MS = 360%
Si	0.5	4,200	2.3	9,660	MS = 400%
Al	0.4	990	2.7	2,670	
Sb	1.1	650	6.7	4,360	
$SnB_{0.5}Co_{0.5}O_3$	0.7	600	3.7	2,220	High irreversible capacity
$Li_{2.6}Co_{0.4}N$	0.8	1,200	2.2	2,640	Unstable in air

[a]Crystallinity $(3.44–d_{002})/0.0868$

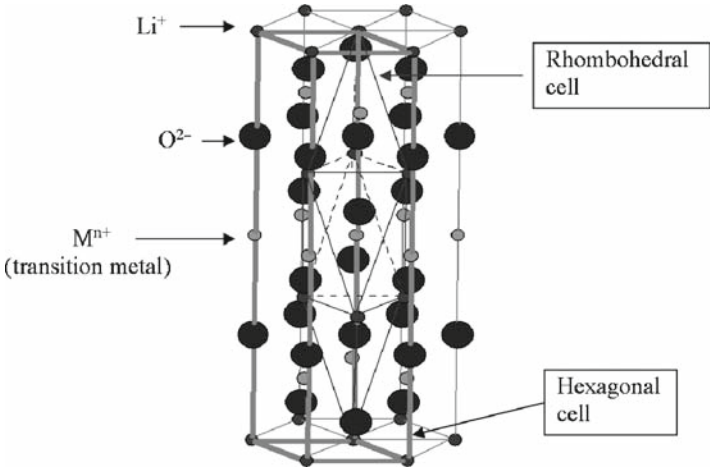

Fig. 2.1 Relation between rhombohedral cell and hexagonal cell

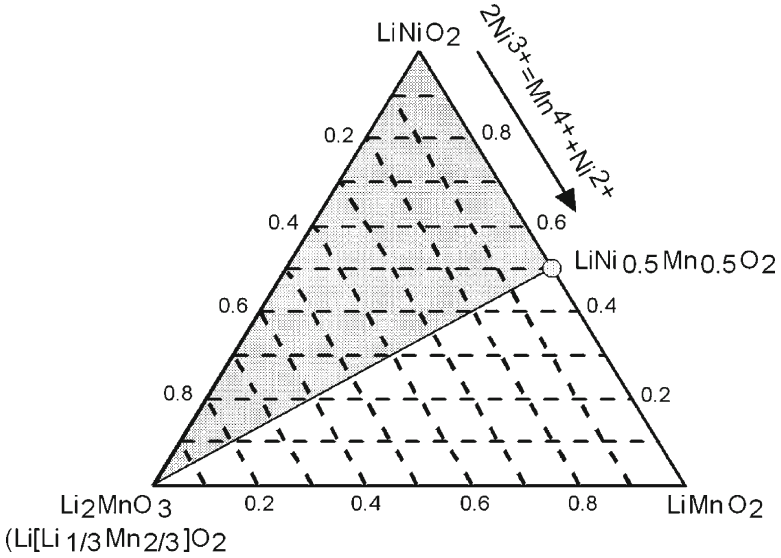

Fig. 2.2 Region of Li_2MnO_3–$LiNi_xMn_{1-x}O_2$ solid solution (painted) in pseudoternary phase diagram

Two types of solid solution are known in the cathode material of the lithium-ion battery. One type is that two end members are electroactive, such as $LiCo_xNi_{1-x}O_2$, which is a solid solution composed of $LiCoO_2$ and $LiNiO_2$. The other type has one electroactive material in two end members, such as $LiNiO_2$–Li_2MnO_3 solid solution. $LiCoO_2$, $LiNi_{0.5}Mn_{0.5}O_2$, $LiCrO_2$, $LiMnO_2$, and $LiFeO_2$ are electroactive end members; on the other hand, Li_2MnO_3, Li_2TiO_3, and $LiAlO_2$ are electrochemically

inactive end members. The combination of two different types of end members gives a lot of cathode materials in lithium ion battery. Solid solutions with more complicated combinations composed of end members are $LiNi_{0.8}Co_{0.15}Al_{0.05}O_2$ or $Li_{1+x}Ni_yCo_zMn_{1-y-z}O_{2+\delta}$.

Among manganese-based layered compounds, a layered zigzag-type orthorhombic $LiMnO_2$ and layered $LiMnO_2$ with R_{3m} symmetry are electroactive materials. The latter is prepared by the ion exchange method[3,4] or by the liquid-phase synthesis.[5] Both orthorhombic and layered $LiMnO_2$s are unstable for electrochemical extraction and insertion of the lithium ion, and they change into a spinel structure during the charge and discharge in 3–4 V range. Orthorhombic $LiMnO_2$ synthesized at high temperatures requires many charge/discharge cycles until the transformation to the electrochemically active spinel structure.[6] However, when it is crushed into nanosized particles, it delivers a capacity close to 200 mAh/g in the first cycle. Further, the cyclability at a high temperature also is excellent,[7,8] and it is in the level that the practical application as a cathode material can be allowed.

A series of compounds with lithium-deficient stoichiometry can be synthesized using the ion exchange method. $Li_{0.7}MnO_2$ analogues are synthesized by ion exchange of the $Na_{0.7}MnO_2$ analogue with the Li^+ ion in the molten lithium salt.[9] $Na_{0.7}MnO_2$ has the stacking faults of the oxygen ion sheets. These faults are partly succeeded by $Li_{0.7}MnO_2$ after ion exchange.

The oxygen ions usually make the cubic or hexagonal close-packing (HCP) structure in metal oxides, and metal ions are located in tetrahedral holes or octahedral holes. In the cubic close-packing (CCP) structure, the oxygen ion sheets are divided into three types (A, B, and C) with different phases, and these layers are stacked regularly in the mode of (ABC)*n* (Fig. 2.3). The stacking mode of the HCP structure is described as (AB)*n*. Two oxygen-sheet stacking is typical in metal oxides. However, $Na_{0.7}MnO_2$ has a different stacking sequence and it is described as (ABBA)*n*. Then, two kinds of the hole with different shapes are formed by six oxygen ions: the octahedron and the prism (triangle pole). The manganese ions occupy the octahedral sites C (between A and B in the oxygen sheet) of the same position on a two-dimensional plane with oxygen sheet C, and the sodium ions occupy the prismatic sites between two A sheets or two B sheets. The structures of $Na_{0.7}MnO_2$ and $LiCoO_2$ occasionally were called P2 type and O3 type in the literature, respectively. The relationships between oxygen and the metals in this notation are shown in Table 2.2, where the positions on the two-dimensional planes A, B, and C are equal to a, b, and c, respectively.

$Li_{0.7}MnO_2$ of O2 structure (O2-$Li_{0.7}MnO_2$) has been prepared from P2-$Na_{0.7}MnO_2$ by the ion-exchange reaction, and O3-Li_xMnO_2 is obtained from P3- or O3-$Na_{0.7}MnO_2$.[10,11] The O2-$Li_{0.7}MnO_2$ keeps its structure during the charge/discharge cycles, although O3-Li_xMnO_2 with R_{3m} symmetry transforms to the spinel structure. The charge/discharge capacity of O2-$Li_{0.7}MnO_2$ is considerably as high as 150 mAh/g in the voltage range of 2.5– 4.0 V, and the capacity in the 3 V range is roughly half; therefore, it is slightly inferior to the 4-V class material in energy density. Various analogues, in which manganese was partly substituted by cobalt, nickel, and so forth, were studied and some of them have higher capacity than the original one. However, they may be ranked as future materials because they have a

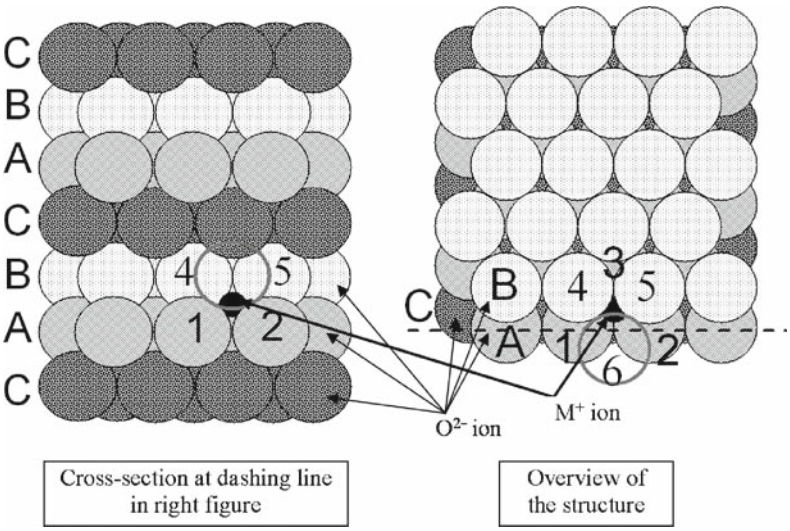

Fig. 2.3 Oxygen stacking in CCP structure

Table 2.2 Relation between oxygen staking and its cation site

Abbreviation	Staking of O^{2-}	Shape of MnO_6	Position of metal[a]	Example
O3	(ABC)*n*	Octahedral	cabcab	$LiCoO_2$
O2	ABCB etc	Octahedral	caac	$Li_{0.7}MnO_2$
O1	(AB)*n*	Octahedral	cc	CoO_2
P3	(AABBCC)*n*	Octahedral and prism	pcp′ap″b	Na_xMnO_2
P2	(AABB)*n*	Octahedral and prism	pcp'c	$Na_{0.7}MnO_2$
P1	(AA)*n*	Prism	pp	–

[a]p, p′, and p″ are different in the position on dimensional plane

poor rate performance; for example, the capacities of $Li_{0.7}Mn_{2/3}M_{1/3}O_2$ (M = Ni, Co) are about 100 mAh/g even at the slow rate of C/20.

It also has been reported that a cobalt-substituted compound (O3-$LiCo_{1/2}Mn_{1/2}O_2$), by the ion exchange method, could be used as the material for the 5-V cathode; however, it has problems such as a large irreversible capacity.

2.3 Electrochemical Characteristics and Structural Changes during Charge/Discharge

2.3.1 Layered Material

The charge/discharge curves of $LiCoO_2$ and $LiNiO_2$ are shown in Fig. 2.4. When the cutoff voltage is selected to be 4.3 V, $LiCoO_2$ has a comparatively smooth curve, while $LiNiO_2$ has a complicated curve with some voltage plateaus. In the following,

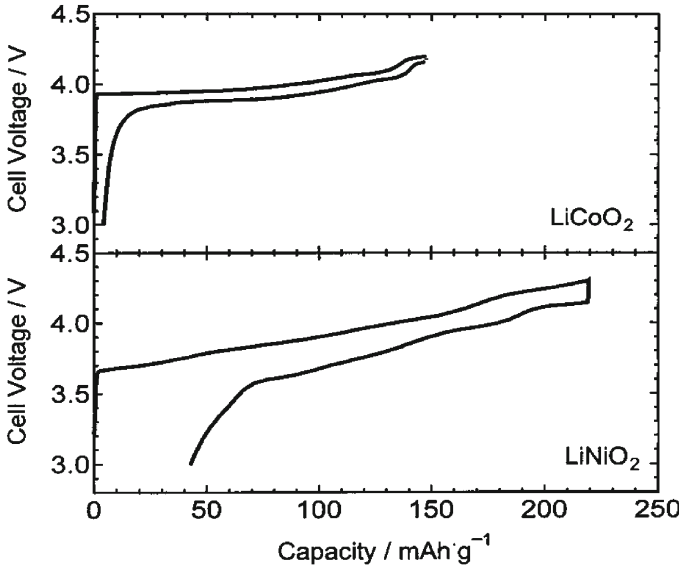

Fig. 2.4 Charge/discharge curves of $LiCoO_2$ and $LiNiO_2$

the composition of the $LiNiO_2$-type compound during the charge/discharge will be expressed as $Li_{1-x}NiO_2$. The origin of this complicated curve is attributed to the structural transformation. $Li_{1-x}NiO_2$ keeps its original structure intially; however, it transforms the monoclinic phase in the range of $0.22 < x < 0.64$. Further delithiation causes the formation of the NiO_2 phase in the range of $x > 0.70$ or more.[12–14] For $LiCoO_2$,[15–17] two crystal phases with R_{3m}^- (original $LiCoO_2$ and $Li_{0.75}CoO_2$) appears in the range of $x < 0.25$. The second rhombohedral phase continues except for a narrow range around $Li_{0.5}CoO_2$, which is a monoclinic phase the same as $Li_{1-x}NiO_2$. However, this phase transforms the rhombohedral phase by increasing the temperature. However, lithium excess $LiCoO_2$ shows different behavior from stoichiometric $LiCoO_2$. It does not have the two-phase range of $x < 0.25$ and the monoclinic phase at around $x = 0.5$, which also is easily judged from the shape of its simple charge/discharge curves. The electrochemical reaction of lithium excess $LiCoO_2$ proceeds in one phase, where the length of the *c*-axis continuously increases and that of the *a*-axis decreases as the degree of the delithiation.[18]

The researchers have reported various values for the formation range of the monoclinic phase and the NiO_2 phase; this would be due to the difference in sample composition because of the easy formation of $Li_{1-x}Ni_{1+x}O_2$ ($x > 0$). The length of the *a*-axis and the cell volume continuously decrease as the degree of delithiation decreases. These changes can be well explained by the reason that the ionic radius of the transition metal decreases as the increase in the oxidation number increases. However, the length of the *c*-axis (interlayer distance) increases as delithiation increases. There are some differences between $LiCoO_2$ and $LiNiO_2$ in the changes

of the length on the *c*-axis in the range of $x > 0.6$, as shown in Fig. 2.5. As for $LiCoO_2$, the length of the *c*-axis has a maximum value and then gradually decreases. On the other hand, for $LiNiO_2$, the interlayer distance becomes constant in the range of $x > 0.6$ or more, and the NiO_2 phase appears in the range of 0.7 or more. The CoO_2 phase is formed for $LiCoO_2$ only in the vicinity of $x = 1$. The structure of layered material during the charge/discharge seems to be quite different between $LiCoO_2$ and $LiNiO_2$, as described previously; however, substitution of 20% nickel by manganese in $LiNiO_2$[19] changes the behavior of the c length to that of $LiCoO_2$. Finally, the lithium content and type of transition metal ion have an extreme influence on the structure of charged layered material.

The upper limit of the monoclinic-forming range ($x = 0.75$) in $LiCoO_2$ roughly coincides with lower limit of the NiO_2-forming range in $LiNiO_2$. If the structure of $Li_{1-x}CoO_2$ in this range has stacking faults,[20] the stacking of the oxygen ion sheets in both $LiCoO_2$ and $LiNiO_2$ changes in the range of $x > 0.7$. The structure change within $x < 0.7$ is due to a slight deviation of the position of atoms; on the other hand, that with $x > 0.7$ causes the change in the stacking of the oxygen sheets. This would be the main reason of poor cyclicity for higher-capacity withdrawing in $LiCoO_2$ and $LiNiO_2$.

The shape of the charge/discharge curves also depends on the stacking of oxygen sheets. The O2–$Li_{0.7}MnO_2$ gives complicated charge curve with several voltage plateaus.[21,22] The stacking of the oxygen sheets changes from (ABCB)*n* to (ABCBCABABCAC)*n* by the extraction of more than 0.5 Li^+, and this structure change causes the shrinkage of interlayer distance.[22]

In the present study, $LiNi_{0.5}Mn_{0.5}O_2$ and $LiCo_{1/3}Ni_{1/3}Mn_{1/3}O_2$ keep R_{3m} symmetry up to $x = 0.62$ [23] and $x = 0.76$,[24] although a discontinuous shrinkage in the length of the *a*-axis accompanies the vicinity of 125 mAh/g of charging ($x = 0.45$). If these compounds do not cause the rearrangement in the stacking of oxygen sheets, we

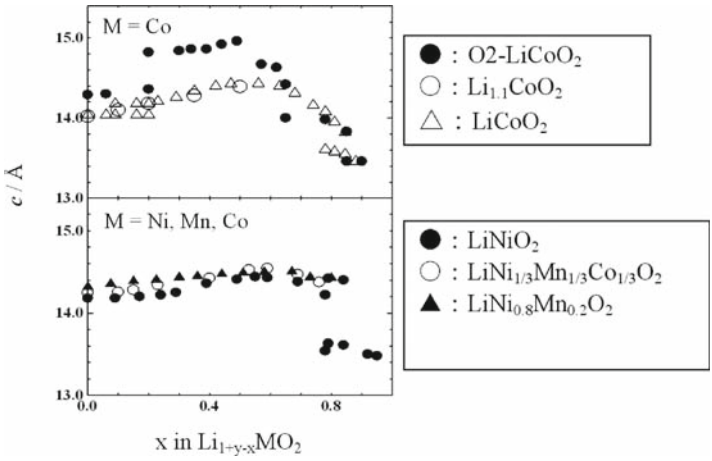

Fig. 2.5 Variation in *c*-axis of layered cathode materials during the charge

could withdraw higher capacities without loss of cycling performance by increasing charge voltage, although decomposition of electrolyte should be overcome.

The O2–$Li_{0.7}Li_{1/18}Mn_{17/18}O_2$ structure obtained from P2-$Na_{0.7}Li_{1/18}Mn_{17/18}O_2$ by the ion exchange method delivers capacities of about 15 mAh/g in the range of 4.0 to 4.5 V and about 130 mAh/g in the range of 3.0 to 3.5 V, respectively.[24] When a part of the manganese ions is substituted with transition metal ions M (Ni, Co, etc.), the capacity of the 3.0–3.5 V range decreases and a new potential plateau appears at 2.5–3.0 V.[9–11] The oxygen structure is kept in all voltage ranges, and an excellent cycling performance is observed at 30°C; however, its cyclicity deteriorates at 55°C.[9]

2.3.2 Spinel

Manganese, whose resource is abundant and inexpensive, is used worldwide as an environmentally friendly and inexpensive dry battery material. Moreover, when a spinel-type manganese-based material is used as the electrode material of a lithium-ion battery, the battery has the advantages of greatly improved safety and an inexpensive battery control circuit. The market trend for the manganese-based cathode material in a lithium-ion battery is roughly divided into two categories. The first category is materials used in portable electronic devices such as the mobile phone. The spinel lithium manganate has been used for the power source of the mobile phone for many years because of its excellent safety and cheaper control circuit,[1] although its market share is low. Moreover, it is said that the capacity fading of the graphite anode during the cycling is prevented by the use of $LiNi_xCo_{1-x}O_2$–$LiMn_2O_4$ mixed cathode because of lower manganese deposition on the anode even at elevated temperatures.

By the way, $LiCoO_2$ has been used mainly as the cathode material in the lithium-ion battery for mobile phones because of high-energy density. However, the rapid rise in price for the lack of the cobalt resources has promoted the hybridization between the cobalt-based material and the manganese-based material with the spinel structure. Further, it has been confirmed that this hybrid material can have the same energy density as that of the conventional one, so the hybrid-type batteries came onto the market since 2004. It is expected that the share of this type of battery will expand further in the future.

The second category is the cathode materials for large-size lithium-ion batteries as power sources for electric vehicles, hybrid vehicles, and so forth. High power, safety, and low cost are strongly required among their performances, so manganese-based cathode materials are suitable for such applications. It overwhelmingly excels in the power density compared to cheaper iron-based cathode material ($LiFePO_4$) and it is used in a large-sized battery. It has been used for 3 years since it appeared in the market as a power source for the hybrid vehicle. Moreover, the spinel-type manganese oxide is used for the main cathode material of the lithium-ion battery for the motor-assisted bicycle and the electric motorcycle, which came onto

the market in recent years. In addition, although the iron-based material ($LiFePO_4$), which is expected to succeed the manganese-based cathode material, is being studied all over the world; it has not reached practical use yet because of its poor electric conductivity and its complicated synthesis method.

It is indispensable for the cathode material to contain redox metal ions and Li ions for delithiation at charging. Higher contents of redox ions and Li ions are desirable to withdraw a high capacity from cathode materials. A material with lower formula weight has the advantage getting higher specific energy density per weight; therefore, the oxygen ion with lower mass per charge and free material cost is the most suitable for the charge compensation of cation. In other words, the lithium- manganese oxides are desirable for the cathode materials in lithium-ion batteries. Spinel-type $LiMn_2O_4$, spinel-type $Li_2Mn_2O_4$,[25] orthorhombic $LiMnO_2$,[26] layered $LiMnO_2$,[27] O_2 type $Li_{0.7}MnO_2$,[28] $Li_{0.33}MnO_2$,[29] and so forth are reported to be such manganese-based cathode materials. $Li_{0.33}MnO_2$ is a 3-V type cathode material with high capacity,[29] which was developed by the authors. The Tadiran Co. in Israel commercialized the AAA-type battery composed of this cathode and metallic lithium anode.[30] This battery has a unique safety mechanism, in which the oxolane acts as both solvent for electrolytes, containing amines as inhibitors for polymerization and monomers for the polymerization when the temperature rises to an emergency level.[30] The active material, composite dimensional manganese oxide (CDMO), developed and commercialized by Sanyo Co., also is considered to be $Li_{0.33}MnO_2$.[31] However, the coin-type cell mainly is used for safety in the application of the secondary battery and it is used as a battery for memory backup. Moreover, spinel $Li_2Mn_2O_4$, layered $LiMnO_2$, and $Li_{0.7}MnO_2$ are prepared by chemical reduction or ion-exchange reaction using an expensive reagent; therefore, the manufacturing cost becomes expensive and the advantage of low material cost is lost. Finally, the remaining candidates for the manganese-based cathode material in the lithium-ion battery will be spinel $LiMn_2O_4$, orthorhombic $LiMnO_2$, and a layered manganese-based material, for instance, the $LiMn_xNi_yCo_{1-x-y}O_2$ and $LiMn_xNi_{1-x}O_2$ type materials. All of them can be synthesized by a simple solid-state method. It has been said that orthorhombic $LiMnO_2$ has a poor cyclicity because its crystal structure changes into spinel at the first stage of charge/discharge; afterward, the charge/discharge reaction proceeds, maintaining the spinel structure although it exhibits a capacity of 200 mAh/g or more in the 3 to 4 V range. However, an orthorhombic manganese material, which has an excellent cyclicity even in the 3–4 V range, also has been reported.[32]

Although the layered Ni–Mn-based cathode material has been placed on the market in the form of single or mixed cathode material,[33–35] here we will explain the spinel manganese-based material. This compound also has been placed on the market in the form of single or mixed with a layered nickel- or cobalt-based material.

2.3.2.1 Nonstoichiometry of Manganese Spinel

It was discovered about 20 years ago that the manganese spinel compound can be oxidized electrochemically. The studies on the manganese spinel at an early stage

were focused on the properties of 3-V class cathode material, and it was clarified that the spinel compound forms a cation-deficient type ($Li_2Mn_4O_9$) or a lithium-excess type ($Li_4Mn_5O_{12}$). Moreover, the authors have clarified that oxygen-deficient spinel compounds are formed in the high temperature synthesis. As mentioned, the lithium–manganese spinel is a complicated nonstoichiometric compound, in which lithium and manganese are distributed in a cubic close-packed structure of oxygen anions. The authors have classified the spinel compounds into the oxygen stoichiometric spinel and the oxygen-deficient spinel whether the close-packed structure of the oxygen ion was maintained or not, and found that the cyclicity of both spinels are remarkably different. The oxygen stoichiometric compounds with an excellent cyclicity as a cathode in lithium ion batteries are composed of three kinds of oxygen stoichiometric spinel: $LiMn_2O_4$, $Li_4Mn_5O_{12}$ (the molar fraction of $Li_{4/3}Mn_{5/3}O_4$ is expressed by x), and $Li_2Mn_4O_9$ (the molar fraction of $Li_{8/9}Mn_{16/9}O_4$ is expressed by y). Such compounds can be expressed by a general formula as $Li_{1+x/3-y/9}Mn_{2-x/3-2y/9}O_4$. It has the excess oxygen if $y > 0$, because the oxygen stoichiometric spinel is constituted by the oxygen-excess type (cation-deficient) $Li_2Mn_4O_9$. The composition of $Li_{1+x/3-y/9}Mn_{2-x/3-2y/9}O_4$ is plotted inside of triangle ABC in phase diagram of Li–Mn–O spinel (Fig. 2.6), where three kinds of oxygen stoichiometric spinels, $LiMn_2O_4$, $Li_{4/3}Mn_{5/3}O_4$, and $Li_{8/9}Mn_{16/9}O_4$, are located at the corner. The vacancy in cation site (8a and 16d) and anion site (32e) is shown by the same symbol, □. The figure is expressed by using two parameters; one is average oxidation number of manganese (m) and lithium–manganese atomic ratio (n) in spinel. These were directly determined by chemical analysis. Spinels on the parallel line against line AC have the same n value and that against line BC have the same m values. The oxygen stoichiometric spinel without oxygen deficiency presents outside of the

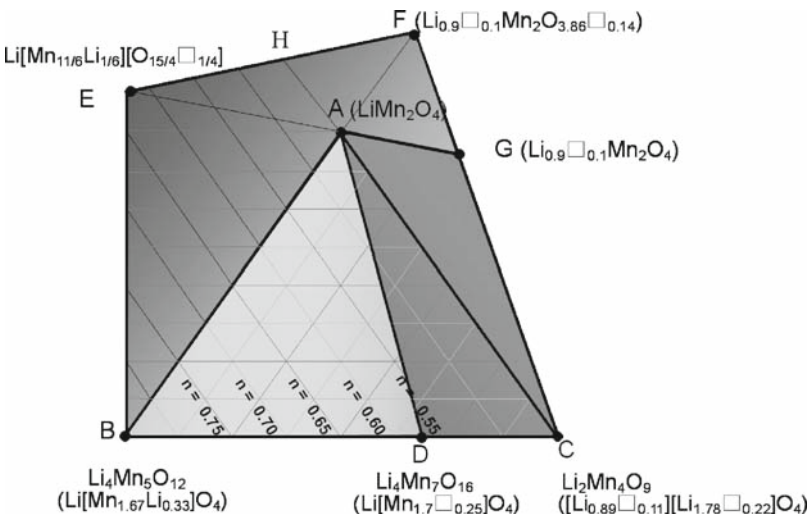

Fig. 2.6 Ternary phase diagram of Li–Mn–O spinels

basic triangle (shown in triangle, AGC), if n is less than 0.5. It is divided into two groups from the structural viewpoint. One is lithium-excess spinel with cation vacancy in only the 8a site (the area of triangle ABD) and the other is the oxygen-excess spinel with vacancy in 8a and/or 16d site (the area of polygon ADCG).

The oxygen-deficient spinels are plotted in the area of polygon ABEFG, where E, F, and G are temporary and hypothetical compounds. Line AG has the relation, $m + n = 4$, and line AE, $3m + n = 11$. Point F is an extrapolation of line AB to $n = 0.45$. The 8a site lithium content is smaller than Mn^{3+} content in the area of triangle ABE and a reverse relation presents in the area of polygon AEFG. The preparation of spinel at higher temperatures causes loss of oxygen; then its composition moves in an upper parallel to AB line with same n values by the heating by higher temperatures or prolonged time. Spinel compounds in the area of polygon AGFH have a vacancy in both cation site (8a) and oxygen site (32e); however, those in the area of triangle AEH have only oxygen deficiency. Pure oxygen-deficient spinels with high crystallinity are scattered around corner A.

The first report on the relation of cycle behavior and oxygen deficiency was reported by Yoshio and Xia in 1997.[36] As will be described later, the fact that the 3.2–3.3 V capacity due to the oxygen-deficient spinel is explained by us[37] and supports that the crystal structure of the oxygen-deficient spinel is the $LiMn_2O_{4-\delta}$ type. However, there were several different opinions for the structure of oxygen-deficient spinels such as: it had no substantial oxygen deficiency but had a structure in which the manganese ion shifted to the 8a site; it had a structure in which the manganese ion shifted to the 16c site; and there was Mn_2O_3 as an impurity, although it could not be detected. The structure in which the manganese ion occupies 8a site would be speculated from the structure of tetragonal spinel Mn_3O_4. When the lithium content decreases and the average oxidation number of manganese approaches 3, the crystal distorts from cubic to tetragonal because of the Jahn–Teller effect of Mn^{3+} as it is frequently said, and the transfer of manganese to 8a site occurs at this time.[34] Kanno et al. have clarified that the structure of cubic spinels is the oxygen deficient-type, using the analysis of neutron diffraction data with high reliability for the sake of its high sensitivity to oxygen and lithium.[38] They have also clarified that there is no cation mixing in the 8a site of oxygen-deficient spinel.[37]

The authors systematically carried out the research about the relation of the oxygen content in the spinel with the battery performance and the structural change in detail for the first time, and found that the battery characteristics of the spinel compounds are considerably dependent on the oxygen content. It was found by this study that some of the poor electrochemical behaviors are not common in spinels but peculiar in the oxygen-deficient spinel. For instance, the spinel compound has been considered to give the capacity fading during the cycling even at room temperature as described in most papers, and this capacity fading was attributed to the Jahn–Teller effect. However, we have elucidated for the first time that above spinel compounds are oxygen-deficient spinels. This will be explained in detail in the following. First, the charge/discharge curves of the oxygen stoichiometric spinel and the oxygen-deficient spinel are shown in Fig. 2.7.[37] Samples in Fig. 2.7a, b are an oxygen stoichiometric spinel $LiMn_2O_{4.02}$ and an oxygen- deficient spinel

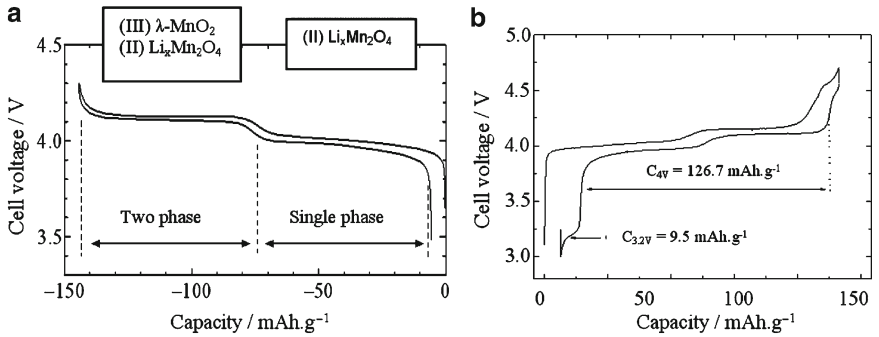

Fig. 2.7 Charge/discharge curves of oxygen stoichiometric spinel (*left*, **a**) and oxygen-deficient spinel (*right*, **b**)

$Li_{1.002}Mn_{1.998}O_{3.981}$, respectively. The 4-V region of $LiMn_2O_{4.02}$ consists of two smooth plateaus: the 4.0-V region (low-voltage plateau) and the 4.15-V region (high-voltage plateau). Here, the charge/discharge product of $LiMn_2O_4$ is expressed as $Li_{1-x}Mn_2O_4$. The low-voltage plateau ($x < 0.5$) is a single-phase region (only cubic II phase exists) where the *a*-axis of spinel $Li_{1-x}Mn_2O_4$ successively shrinks as the increase in x. The high-voltage plateau ($x > 0.5$) is a two-phase region where two cubic phases with different lattice parameter, $Li_{0.5}Mn_2O_4$ (cubic II phase) and λ-MnO_2 (cubic III phase), coexist. On the other hand, the oxygen-deficient spinel, for instance $Li_{1.002}Mn_{1.998}O_{3.981}$, have extra voltage plateaus at around 3.2 V and 4.5 V in addition to the high-voltage plateau and the low-voltage plateau in the discharge curve. The electrochemical reaction is different from that of the oxygen stoichiometric spinel in the low-voltage plateau, it becomes a two-phase mechanism where cubic I and cubic II phases exist.[39] The capacity fading during the cycling is liable to occur because the charge/discharge process accompanies the phase transition in the two-phase region. Figure 2.8 shows the relations between the amount of oxygen deficiency and the cyclicity at room temperature for the spinel compound. Since a linear relation is observed between the amount of oxygen deficiency (δ) and the capacity retention percent, it is clear that the oxygen deficiency dominates the cyclicity at room temperature. Moreover, the extrapolated value of the capacity retention to $\delta = 0$ becomes 100%, and it indicates that the room temperature capacity fading during the cycling does not occur without the oxygen deficiency. Based on the above discussion, it will be understood that the capacity fading of the oxygen-deficient spinel during the cycling even at room temperature is attributed to two sets of the two-phase reaction in both the high- and low-voltage plateaus.

In addition, the capacity fading during the cycling occurs in a simple oxygen stoichiometric spinel because the two-phase reaction proceeds in the high-voltage plateau; however, it is not so serious compared to that in the oxygen-deficient spinel. In other words, the reason for residual capacity fading of the oxygen stoichiometric spinel is the formation of λ-MnO_2 phase (cubic III) at deep delithiation. Finally, if deep delithiation of spinel is inhibited, an electrochemical reaction would proceed under the single-phase mechanism over all of the 4-V range and the cyclicity would

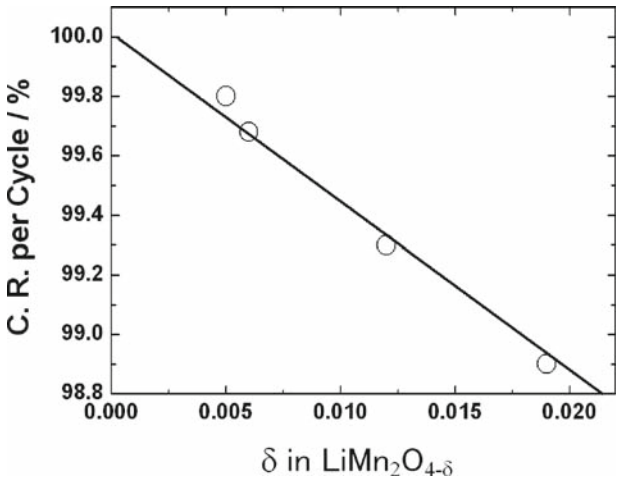

Fig. 2.8 The relation between amount of oxygen deficiency (δ) and capacity retention per cycle (CR per cycle) at room temperature

be improved. The authors have already indicated that it is easily overcome by use of lithium-excess spinel $Li_{1+x}Mn_2O_4$ without oxygen deficiency.[40]

However, oxygen-deficient spinels are formed easily when lithium-excess composition is selected. Such a problem is easily solved by doping foreign metal ions, which accelerates the formation of oxygen-excess-type spinels. In the other words, the oxygen stoichiometric spinels are easily formed using the above doping technique even for lithium-excess composition. The amount of the cation deficiency for foreign metal-doped spinel was estimated from the relations between the amount of the doped metal ion and the capacity (although it depends on the synthesis temperature). These are determined to be 1% for chromium, 1–1.5% for cobalt and aluminum, and 1.5–2% for nickel-doped spinels, and it is confirmed that the foreign metal ion doping promotes the formation of the oxygen stoichiometric spinel. The formation of oxygen deficiency in spinels cannot be neglected for the preparation at ca. 800°C even in the case of the foreign metal doping. Consequently, an excellent synthesis method is desired to fulfill two conditions, i.e., oxygen stoichiometry and prevention of λ-MnO_2 formation at a charged state. The detection of 3.2-V plateau in the discharge curve is convenient to confirm the presence of oxygen deficiency in the spinel compound.

By the way, the battery manufacturers have recommended the high-temperature synthesis to get spinels with lower specific surface area, because they believed the statement in the paper[41] that the capacity fading during the cycling especially at the elevated temperature is dependent on the dissolution of manganese from spinel compounds. As a result, the oxygen-deficient spinel had been offered to the companies, and the physicochemical and electrochemical characteristics of such spinels had been measured. Then, the characteristics of the spinels reported in an earlier study were those of the oxygen-deficient spinel, and such reports gave extreme

misunderstandings for the characteristics of the spinel. These misunderstandings are enumerated as follows:

1. The spinel deteriorates during the cycling.
2. The largest deterioration occurs at a depth of discharge of 60–100%,[42] based on the measurement about the effect of storage time on the capacity fading at various discharge depths.
3. The spinel compound changes its structure when it is cooled below the room temperature.[43]

It should be noted that all these descriptions concern the oxygen-deficient spinel and cannot be adopted to the oxygen stoichiometric spinel. That is, it is not overdone how strongly it is emphasized that the oxygen stoichiometric spinel does not have these three features. As mentioned above, it should be understood for the spinel compounds that the data of spinels, in which oxygen content is measured by the chemical analysis, would be reliable.

2.3.2.2 Stabilized Spinel Compounds

As previously described, the synthetic conditions for an excellent spinel compound are considerably restricted. First, it should be an oxygen stoichiometric compound. Second, doping of different kinds ions including Li^+ ion is required in order to proceed the to the charge/discharge process under the single-phase reaction throughout the 4-V region. The chemical composition of desirable spinels is described to be $Li_{1+x}M_yMn_{2-x-y}O_4$. It will be necessary for such spinels to keep roughly $0 < x < 0.06$ and $0.03 < y < 0.15$ in order to withdraw the discharge capacity of around 100 mAh/g. Here, M is one or more kinds of metal ion excluding Li^+ ion. If the counterelectrode is metallic lithium, the cyclicity of the spinel compound is excellent even in the electrolyte of about 60°C. However, it is well known that the insertion and extraction of Li^+ ion for the graphite anode are obstructed by deposited mangnanese from the dissolved manganese ion in the lithium-ion batteries. Since the dissolved manganese ion causes deterioration in the cyclicity of the graphite anode, the performance of the lithium-ion battery also causes deterioration by the influence of the anode.[44] As this deterioration phenomenon of the anode is particularly remarkable in the high temperature electrolyte, the third condition to decrease the concentration of the dissolved manganese ion is required.

The authors have developed a new method (two-step heating; initial firing at 900–1,000°C and second refiring at 600–800°C) for synthesizing the spinel-type cathode material. We have succeeded in the preparation of spinels, which satisfy the above three conditions at the same time.

Well-developed spinel crystallines with lower specific surface area are formed in the initial firing process. Such lower specific surface area is very effective to reduce the amount of manganese dissolution into the electrolyte. It is proven by the chemical analysis that the oxygen-deficient spinel absorbed oxygen and changed to the oxygen stoichiometric spinel in the second refiring process. However, it is

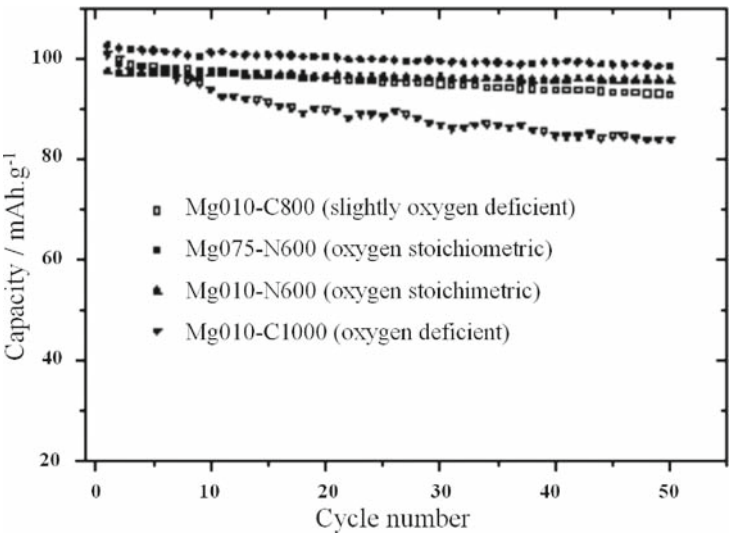

Fig. 2.9 Cycling performance of Mg-doped spinels at 60°C. Mg010-C800: oxygen-deficient $Li_{1.035}Mg_{0.093}Mn_{1.873}O_{3.99}$; Mg075-N600: oxygen stoichiometric $Li_{1.034}Mg_{0.080}Mn_{1.886}O_{4.010}$; Mg010-N600: oxygen stoichiometric $Li_{1.036}Mg_{0.10}Mn_{1.864}O_{4.021}$; Mg010-C1000: oxygen-deficient $Li_{1.033}Mg_{0.090}Mn_{1.877}O_{3.997}$

important in first process to prepare the spinel, in which the amount of oxygen deficiency is as small as possible for the sake of easy conversion to the oxygen stoichiometric spinel in the second process. In that case, it has been found that the magnesium ion, the aluminum ion, the nickel ion, and the cobalt ion are preferable for doping metal ions.

Figure 2.9 shows the cyclicity of the magnesium doping spinel cathode for metallic lithium anode at 60°C.[45] It is understood that the cyclicity of the oxygen stoichiometric spinels is excellent.

In the case of spinel compounds prepared at about 1,000°C with this method, the concentration of manganese ion is roughly 3 ppm even when spinels are stored in the electrolyte at 60°C for 4 weeks. Such value is significantly lower than 100 ppm of $LiMn_2O_4$ prepared at 800°C. Finally, manganese dissolution from spinel can be reduced about 1/30 by the introduction of the initial heating process. As a result, the elevated temperature characteristics of the lithium-ion battery composed of the spinel cathode synthesized by this method and graphite anode are considerably improved, as shown in Fig. 2.10.

2.3.2.3 Structure of Manganese Spinel

In spinel $LiMn_2O_4$, the light element, lithium, occupies the tetrahedral 8a site and the heavy metal element, manganese, occupies the octahedral 16d site; O^{2-} (32e site) forms the cubic close packing. The spinel of such a construction is called a

normal spinel. When a foreign metal ion is doped, most of the first transition metal ions substitute for manganese in the16d site, and the crystal becomes normal spinel. However, the zinc ion or the iron ion substitutes for the 8a site according to the synthesis condition, and a random spinel in which the heavy metal element occupies a part of the 8a site is formed.[46] In addition, the gallium ion substitute both the 8a and 16d sites.[47] The interesting point of the zinc-doped spinel is that it forms a cubic structure with the space group P_{4132} in the case of slow cooling and causes the change in XRD pattern as shown in Fig. 2.11, where an additional five peaks in $2\theta°=15°–25°$ are clearly observed. Although manganese-based inverse spinel, in which the heavy metal ion completely occupies 8a site, is not known, $LiNiVO_4$ and $LiCoVO_4$ can be classified into inverse spinel in the cathode material for the lithium battery and the V ion occupies the 8a site.[48,49] The diffusion path of the lithium ion

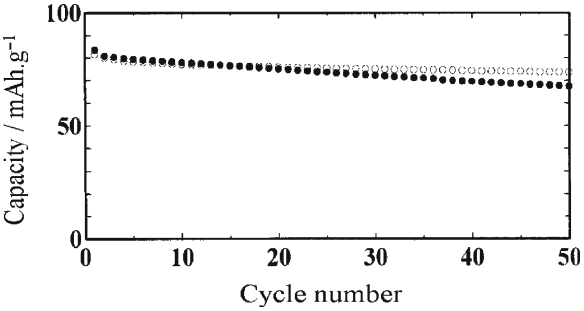

Fig. 2.10 Cycling performance of lithium-ion battery composed of oxygen stoichiometric $Li_{1.06}Al_{0.15}Mn_{1.78}O_4$ and graphite (MCMB6–28) at RT(*open circle*) and 60°C (*filled circle*). Electrolyte contains vinylene carbonate. EC:MEC(3:7), 1-M LiPF6, 4.2–3.3 V

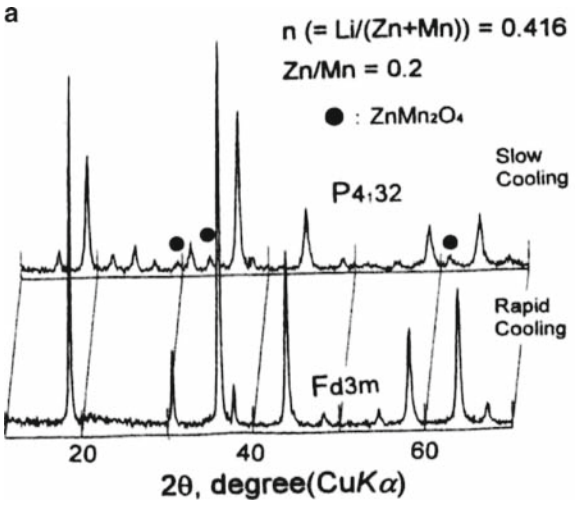

Fig. 2.11 XRD patterns of ordered (P_{4132}) and disordered zinc-doped spinel (F_{d3m})

in this spinel is restricted to the route, such as the octahedral 16c site—the tetrahedral 48f site delithiated 16d. This difficulty in the diffusion of Li^+ ion is considered to restrict the capacity less than 50 mAh/g. In addition, the 8a site where the Li^+ ion exists shares its plane with four 16c sites in the normal spinel, and the Li^+ ion can easily shift from the 8a site to the 16c site.

2.3.2.4 Capacity of Spinel Compound

The authors have confirmed that the measured capacity of the oxygen stoichiometric spinel compound coincides with the capacity calculated from the Mn^{3+} ion content, which was experimentally obtained by chemical analysis within an experimental error. Further, we have established the equations for calculation of capacity from the composition of spinel compounds using the lithium–manganese ratio (n) and the average oxidation number of manganese (m), which are determined experimentally.[36,40,49–52] The classification of spinel compounds, the spinel formula, and the equations for the calculation of theoretical capacity are shown in Table 2.3. The oxygen stoichiometric spinel is classified into the lithium-excess spinel and the oxygen-excess spinel, based on the difference in the site of the cation vacancy. However, the ratio of the Mn^{3+} ion/total Mn above two spinel is commonly described as $(4 - m)/(m + n)$; both equations for the theoretical capacity become equal. On the other hand, the same equation for the capacity is applicable even for the oxygen-deficient spinels with $n<0.5$ and $4\leq m+n$. Two types of oxygen-deficient spinels with different chemical formulas would form. One type of spinel can be described as the formula of $M_3O_{4-\delta}$ (M is arbitrary cation), which has a deficiency only in the oxygen site. The other would be described as the formula of $Li_{1-z}Mn_2O_{4-\delta}$ ($z>0$), which has additional cation deficiency in the 8a site because manganese occupies only the 16d site in the oxygen-deficient spinel. If the electrochemical oxidation of the spinel compound accompanies the oxidation of Mn^{3+} to Mn^{4+} and the release of the Li^+ ion for the charge compensation, then the capacity

Table 2.3 Classification, spinel formula, and capacities of spinel Li–Mn–O compound[a,b]

Classification		Spinel formula	4 V capacity
Oxygen stoichiometric spinel	Lithium excess spinel	$Li[Mn_{8/(n+m)}Li_{(7n-m)/(n+m)}\square_{(3m-5n-8)/(n+m)}]O_4$ $m/7 < n < (3m-8)/5$, $3.5 < m < 4.0$	$1184(4-m)/(m+n)$
	Oxygen excess spinel	$Li_{8n/(n+m)}\square_{(m-7n)/(n+m)}[Mn_{8/(n+m)}\square_{(2n+2m-8)/(n+m)}]O_4$ $n \leq m/7$, $4.0 < m + n$	
Oxygen-deficient spinel	Mn^{3+} lack type	$Li[Mn_{3/(n+1)}Li_{(2n-1)/(n+1)}]O_{3(m+n)/2(n+1)}\square_{(8+5n-3m)/2(n+1)}$ $n > (3m-8)/5$, $3m + n > 11$	$1184(4-m)/(m+n)$
	Li^+ lack type	$Li[Mn_{3/(n+1)}Li_{(2n-1)/(n+1)}]O_{3(m+n)/2(n+1)}\square_{(8+5n-3m)/2(n+1)}$ $n > (3m-8)/5$, $3m + n < 11$	148
		$Li_{2n}\square_{1-2n}[Mn_2]O_{m+n}\square_{4-m-n}$ $n < 0.5$, $4.0 < m + n$	$296n$

[a]□:Vacancy

[b]Formula weight and Mn content are conventionally assumed as same as those of $LiMn_2O_4$

of spinels would be controlled by the Mn^{3+} content or Li^+ content in the spinel; here, we believe Li^+ in the 8a site is electrochemically active.

We can divide the oxygen-deficient spinel for its capacity. The Mn^{3+} content would control the capacity of one type of oxygen-deficient spinel; the capacity is expressed same equation as the oxygen stoichiometric spinel previously mentioned. If the lithium content in the spinel restricts the capacity, although experimental verification has not been carried out, the capacity of such a spinel would be calculated to be 296*n*.

The oxygen-deficient spinels have two equivalent additional discharge plateaus at 3.2 V and 4.5 V. It already has been experimentally confirmed that the relationship, $C_{3.2\,V}(\text{mAh/g}) = 444\delta$, exists between the amount of oxygen deficiency, δ, and the capacity at 3.2 V, $C_{3.2\,V}$ (Fig. 2.12). This capacity can be explained by the participation of five O^{2-} ion-coordinated Mn (MnO_5) from the crystallographic viewpoint as follows. Three manganese ions and one lithium ion surround an oxygen anion, and three MnO_5 are formed when an oxygen ion is lost, i.e., formation of one vacancy as shown in Fig. 2.13. Three MnO_6 octahedra bond to three MnO_5, sharing their edges. The redox potential of all 12 Mn would be changed and generate new voltage plateaus at 3.2 V and 4.5 V. Here, we consider the capacity of oxygen-deficient spinels. The capacity for six Mn^{3+} ions per one oxygen deficiency (half of 12 Mn) is reflected by the total capacity of 3.2 V and 4.5 V. The formation of the oxygen deficiency in $LiMn_2O_4$ can be expressed by

$$LiMn_2O_4 = LiMn_2O_{4-\delta} + \delta/2O_2 \tag{2.1}$$

For a 1-g sample of $LiMn_2O_{4-\delta}$ (formula weight: F_w), the mole of the oxygen deficiency in this sample is δ/F_w. Therefore, the mole of the Mn^{3+} ion that is influenced by the oxygen deficiency becomes $6\delta/F_w$. If δ is small, the value of F_w in $LiMn_2O_{4-\delta}$ can be approximated by the formula weight of $LiMn_2O_4$, and the total capacity of

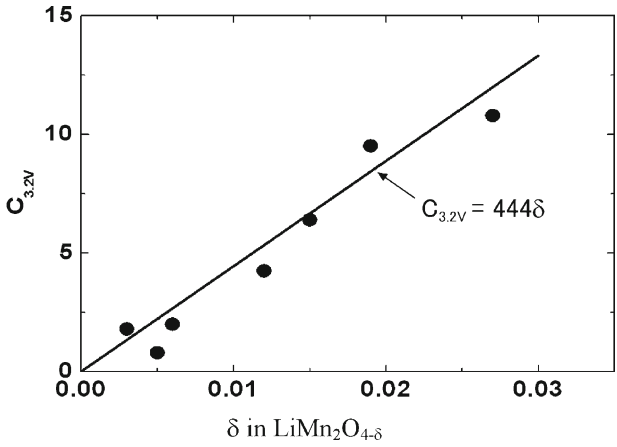

Fig. 2.12 The relation between $C_{3.2\,V}$ and δ in $LiMn_2O_{4-\delta}$

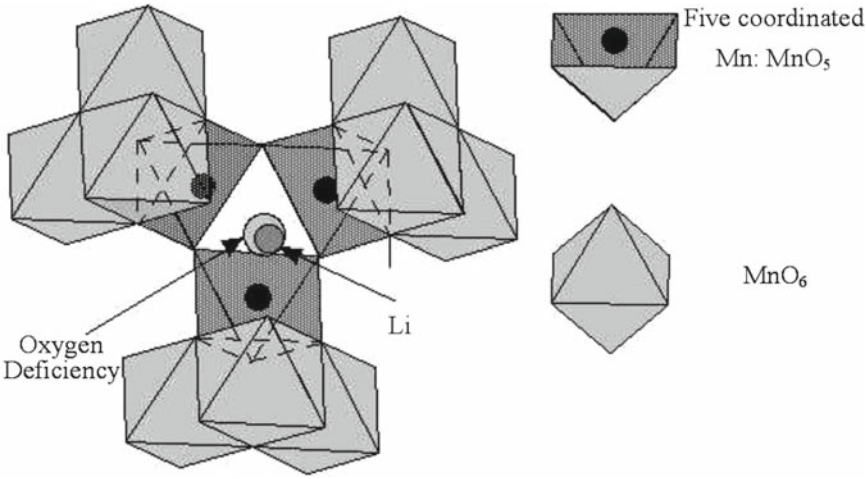

Fig. 2.13 Local structure around oxygen deficiency

3.2-V and 4.5-V region is $6\delta \times 148$ mAh/g = 888δ mAh/g, and one half of it corresponds to the 3.2-V capacity of 444δ mAh/g.

In the spinel material used as a cathode material, the cyclicity is improved by preventing the formation of the λ-MnO_2 phase, and the electrode reaction at a high voltage plateau is changed to the single-phase reaction by introducing the Li^+ ion and the foreign metal ion into the 16d site. However, the control of the composition of the 16d site decreases the Mn^{3+} ion content and causes a decrease in capacity. Here, the capacity of spinels with the ratio of lithium/other metals = 0.5 will be explained. The chemical formula of the oxygen stoichiometric spinel containing foreign metal (M) can be expressed as $Li_xM_yMn_{3-x-y}O_4$ in such cases. Here, the atomic ratio M/(Mn + M) is defined by f [= $y/2$]. When the formula weight of this spinel is approximated by the formula weight of $LiMn_2O_4$, the capacity C (mAh/g) per 1 g of the foreign metal-doped spinel can be calculated using the mole of the Mn^{3+} ion in 1 g of spinel. Then, it can be expressed by (2.2),[52,53] where the charge of foreign metal ion (M) is expressed as v^+:

$$C(\text{mAh/g}) = 148[1-3s-(4v)f] \tag{2.2}$$

That is, the smaller the charge of the foreign metal ion and the larger the f, the capacity decreases. The composition of the spinel can be designed to calculate the biggest capacity, where cation vacancy, s, is equal to zero.

In an ideal 5-V spinel cathode material, the manganese ion is tetravalent[54] and the redox species are foreign metal ions. Nickel, copper, iron, cobalt, and chromium are known as a foreign metal M.[55] The highest 5-V capacity is obtained for the composition of $LiM_{0.5}Mn_{1.5}O_4$ and $LiMMnO_4$, where M is divalent and trivalent, respectively. Although a capacity of 145–147 mAh/g can be expected for the divalent metal (Ni, Cu) under the two-electron transfer mechanism, only $LiNi_{1/2}Mn_{1.5}O_4$

exhibits a discharge capacity of ca. 140 mAh/g in the 5-V region. Although a voltage plateau at the 4-V region based on $Mn^{3+/4+}$ due to the formation of oxygen deficiency appears in this spinel, the introduction of the oxygen absorption process for repairing the oxygen deficiency (annealing under the oxygen atmosphere) is an important technology for increasing the 5-V capacity.[56,57] In the spinel substituted by iron, cobalt, and chromium, the ideal composition with the highest capacity is $LiMMnO_4$ because all three kinds of metals exist as trivalent. Although any samples cannot exhibit a capacity of more than 100 mAh/g in the 5-V region, $LiCrMnO_4$ has no 4-V region because of the absence of oxygen deficiency.

2.3.2.5 Charge/Discharge Mechanism

As it has been already described, it is important for maintaining an excellent cyclability in spinels to keep single-phase mechanism over all 4 V region. Therefore, it is very important to elucidate the charge/discharge mechanism. Two types of reactions are reported for the electrochemical reaction of Li in spinels: The one is the single phase mechanism, where the unit cell simply shrinks or expands during charge or discharge. The other is the two-phase reaction, where two different crystal phases coexist and the ratio of both crystal phases changes. The differences between these two electrochemical reactions are observed in the open circuit voltage (OCV) and the X-ray diffraction profiles. The OCV curve in two-phase mechanism should give flat shape, however, it might give S type curve even in case of the measurement under the non-equilibrium state, and it is likely to misidentify as a single-phase mechanism. Moreover, in the XRD measurement using the CuKα line (two kinds of wave lengths of $K_{\alpha 1}$ and $K_{\alpha 2}$ are irradiated) etc., two diffraction lines of original and produced spinel with closed lattice parameters in the two-phase mechanism are duplicated, and they are regarded as a broad diffraction line. Finally, it might be misunderstood as a single-phase mechanism. Analysis of XRD with high accuracy is possible to use a synchrotron light because monochromatic X-ray with high intensity is obtained. It has been already clarified for the first time by the authors' joint research that the charge/discharge mechanism of the oxygen deficient spinel in the low voltage region is a two-phase reaction.[39]

Figure 2.14 shows the changes in the cubic lattice parameter during the charge for three typical spinel compounds. The reaction of $LiMn_2O_4$ consists of a single-phase reaction in the low-voltage plateau, where the lattice parameter continuously decreases, and a two-phase reaction in the high-voltage plateau, where two cubic phases with different lattice parameters exist. In the oxygen stoichiometric spinel of the metal ion doped-type or the lithium excess type, electrochemical processes at both high-voltage plateaus and low-voltage plateaus proceed in a single-phase mechanism, and the lattice parameter continuously changes. On the other hand, in the oxygen-deficient spinel, two crystal phases with different lattice parameters exist for both low-voltage plateaus and high-voltage plateaus. That is, the cubic phase I of a lattice parameter 8.25 Å and the cubic phase II of 8.17 Å exist in the low-voltage plateau, and it only becomes cubic II at $x = 0.5$. In addition, the cubic

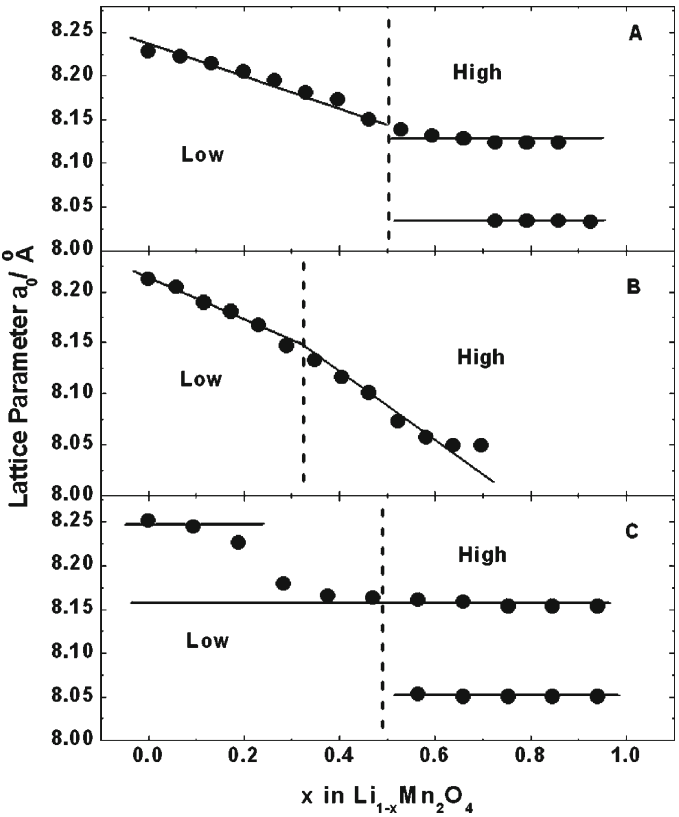

Fig. 2.14 Lattice parameters of delithiated stoichiometric $LiMn_2O_4$ (**a**), oxygen stoichiometric spinel (**b**), and oxygen-deficient spinel (**c**)

phase III of 8.06 Å is formed when the delithiation proceeds, and the crystal phases of cubic phase II and III coexist. The ratio of cubic phase III increases as the delithiation proceeds.

The similar lattice change of such an A type and C type in Fig. 2.14 are reported even for a 5-V cathode material such as $LiNi_{0.5}Mn_{1.5}O_4$.[58] The electrochemical reaction in both low- and high-voltage plateaus are considered to be the two-phase reaction the same as in the oxygen-deficient spinel (C). That indicates the possibility of existence of the oxygen deficiency in the sample used in that report.

2.3.3 Olivine Compound

Orthorhombic $LiFePO_4$ of the olivine structure forms $FePO_4$ during charging/discharging, and two crystal phases exist during charging/discharging; thus it exhibits a flat discharge curve.[59] The accurate crystal structure of orthorhombic

$FePO_4$ formed by charging was obtained using the Rietveld method.[60,61] Substitution of iron by manganese transforms the shape of the charge/discharge curves. The capacities of the lower (3.5 V) and higher voltage region (4.0 V) correspond to the content of iron and manganese. Therefore, a manganese substitution is effective to increase the energy density. However, it causes the decrease in conductivity, which leads to poor rate performance.

2.4 Problems of Cathode Materials (Safety Problem of Layered Material and Spinel $LiMn_2O_4$ Type Materials)

2.4.1 Layered Materials

The cathode materials of lithium batteries have a strong oxidative power in the charged state as expected from their electrode potential. Then, charged cathode materials may be able to cause the oxidation of solvent or self-decomposition with the oxygen evolution. Finally, these properties highly relate to the battery safety.

The self-decomposition reaction of the charged products in $LiCoO_2$ and $LiNiO_2$ is examined in detail using the thermal analysis and the X-ray diffraction method. The thermal decomposition reaction of electrochemically delithiated $Li_{1-y}CoO_2$ ($0.4 < y < 0.6$) is simple, for example, when $y = 0.5$, the reaction obeys the (2.3) and (2.4), and $LiCoO_2$ and Co_3O_4 are observed to be the decomposition products.[62] On the other hand, it is more complicated in $LiNiO_2$. The crystal structure at the charged state becomes rhombohedral or a monoclinic phase, depending on the charged state and the composition of the sample. $Li_xNi_{1-x}O$ with the rock salt structure from $Li_{1-y}NiO_2$ is formed at $y > 0.7$,[63] and a layered product is formed via a spinel phase at $y < 0.7$.[64] The reaction process for $y = 0.5$ is indicated in (2.3) and (2.4). However, it is difficult to determine whether the spinel phase is formed or not because of the similarity in XRD patterns of the spinel and layered structure. Although the formation of the spinel phase is easy in the nickel-excess-type compound,[65] it would be difficult to form $LiNi_2O_4$ in a short time during the thermal analysis by transformation of $Li_{0.5}NiO_2$ to $LiNi_2O_4$, which requires tens of hours in high purity $LiNiO_2$.[66] The difference between both reactions in $Li_{0.5}NiO_2$ is the presence of oxygen evolution; therefore, the oxygen evolution is judged from the weight loss of thermogravimetry:

$$Li_{0.5}\,CoO_2 = 1/2\,LiCoO_2 + 1/6Co_3\,O_4 + 1/6O_2 \tag{2.3}$$

$$Li_{0.5}\,NiO_2 = (1/2\,LiNi_2\,O_4) = 3/2\,Li_{0.33}Ni_{0.67}O + 1/4O_2 \tag{2.4}$$

The main difference between the above two equations is the amount of evolved oxygen gas. Since $Li_{0.5}NiO_2$ release 1.5 times of O_2 than $Li_{0.5}CoO_2$, $LiNiO_2$ has a greater possibility to generate heat than $LiCoO_2$.

Thermal analysis of the charged product without electrolyte gives information only about self-decomposition; then we can know the thermal property of the decomposition reaction, the oxygen-releasing temperature, and the amount of released oxygen. However, thermal runaway in a charged cell is caused by an endothermic reaction between electrolyte and evolved oxygen; measurements concerning the safety of the cell should be evaluated in the presence of an electrolyte.

Dahn et al.[67] have evaluated the heat generation of various charged cathode materials in the presence of an electrolyte by DSC measurement. These data for various cathode materials are summarized in Figs. 2.15a, b in order to understand the relation of the charging capacity with the heat generation and its rate. The total heat generation increases with an increase in the charging capacity for all cathode materials. Plots of 4-V class cathode materials, $LiCoO_2$, $LiNiO_2$, $LiMn_2O_4$, and $LiNi_{0.8}Co_{0.2}O_2$, roughly lie on a straight line in Fig. 2.15. No extreme deviation is observed among 4-V class cathode materials except for $LiNi_{3/8}Co_{1/4}Mn_{3/8}O_2$. The 3-V class $LiFePO_4$ shows lower heat generation. It would be due to its lower oxidative power or stability of a strong covalent bond in PO_4^{3-}. The behavior of $LiNi_{3/8}Co_{1/4}Mn_{3/8}O_2$ is strange. It shows extraordinary lower total heat generation.

These data would guarantee excellent thermal stability of $LiNi_{0.5}Mn_{0.5}O_2$-based cathode materials, such as $LiNi_{1/3}Co_{1/3}Mn_{1/3}O_2$.

$LiNiO_2$ exhibits uniqueness for the rate of heat generation, i.e., the rate of heat generation suddenly increases at the composition of $Li_{0.3}NiO_2$, which contains a NiO_2 phase. Therefore, if the formation of NiO_2 phase is protected, a sudden increase in the heat generation rate would be protected. In fact, the rate of heat generation greatly decreases cobalt doping by 20%. Many researchers[67,68] have reported excellent effects of cobalt doping into $LiNiO_2$ on the thermal stability. It also is reported that the safety of $LiNiO_2$ is greatly improved by the substitution of 1/4Ni by Al.[69] Since the reaction between charged electroactive material and the

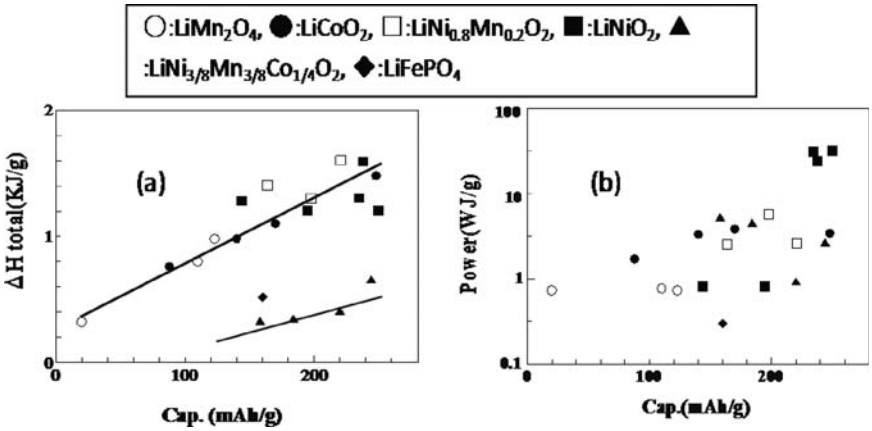

Fig. 2.15 Relation between charge depth and heat generation (**a**) or its power (**b**) for various cathode materials

electrolyte occurs at the interface, the decrease in the particle size of electroactive material causes the increase in the rate of heat generation.[70] Therefore, it is dangerous to use nanosized particle to improve rate capability.

The evaluation of safety for the cathode material also is carried out in the polymer battery system. The $Li_{0.6}CoO_2$, $Li_{0.6}NiO_2$, and $Li_{0.23}Mn_2O_4$ have exothermic peaks of about several W/g in the range of 200 to 300°C[71]; therefore, the reaction between the organic materials and the oxygen generated by the thermal decomposition of cathode material is basically inevitable. In addition, details in the evaluation of safety on lithium-ion batteries are referred to in the paper by Tobishima et al.[72]

2.5 Recent Progress in Practical Cathode Materials for Lithium-Ion Batteries

The battery characteristics, capacities, densities, shapes of the charge/discharge curves, and problems of typical cathode materials, which are used or developed for the lithium-ion battery, are listed in Table 2.1. The $LiCoO_2$ has more than a 90% share in the market of cathode material for the lithium-ion battery, which is applied to cellular phones and portable computers. It has been used since this battery was developed. Manganese-based materials have a share of residual several percent.

The most important factor for a battery is how to increase the active material in the cell with the limited volume. Therefore, the capacity per unit volume is a key factor. The cobalt-based material is still a promising material because an 808 mAh of capacity per unit volume is achieved for the sake of its higher density. Moreover, the shape of the discharge curve also is important because the design of the electric circuit for the charge/discharge control of battery is easier for its sloped curve.

The capacity of lithium-ion batteries has been increased by the improvement of the carbon anode in the initial stage; however, recent improvements in capacity are achieved by the increased charge voltage. Doping foreign ions into $LiCoO_2$ allows the use of a higher charge voltage without capacity fading.[1,73–75] The current 18650-type battery with aluminum- or magnesium-doped $LiCoO_2$ cathode can deliver the capacity of higher than 2.4 Ah.

The practical application of nickel-based materials with large capacity per unit volume has been delayed from the viewpoint of safety; however, the safety of the foreign metal-doped $LiNiO_2$ was confirmed and the practical use of the nickel-based cathode started in fiscal year 2004.

By the way, spinel $LiMn_2O_4$-type materials exhibit excellent safety, so it is considered to be a promising candidate for large-sized batteries such as for hybrid electric vehicles (HEV) and electric vehicles (EV). Battery modules for HEV can be prepared only by connecting ten single cells with the capacity of ca. 10 Ah in series. A lightweight laminated-type battery is suitable for such an application, and the battery price will become more inexpensive. A laminated-type battery containing the manganese-based material appeared in the market as a power source for the motorcycle (metal casing) and the motor-assisted bicycle in 2002. This type battery

came into practical use as the power source for HEV in 2003. Capacity fading of a manganese-based cathode at elevated temperatures has been overcome; it then is almost definite that the manganese-based materials will be used for this type of battery. Magnesium- and aluminum-doped spinels, which have the lowest tendency to form oxygen-deficient compounds, are used mainly.

In Sect. 2.5.1 the design policy of the cobalt-based material used for more than 10 years is described in detail. The changes of design policy, which depends on the safety or charge/discharge conditions of battery, are examined and the current states of nickel- and manganese-based materials, which will appear in the market within 1–2 years, are described.

2.5.1 Recent Cobalt-Based Materials

The lithium-ion secondary batteries appeared on the market in 1990. The anode material was changed later from hard carbon to graphite; however, the cathode material is consistently $LiCoO_2$. Battery-processing technologies also have been improved and the capacity has been improved by about three times during its history. However, the progress in $LiCoO_2$ should not be neglected. Recently, the properties of $LiCoO_2$ have been considerably improved to fit the pulse discharge with high current, which is demanded for recent cellular phones.

First, let us consider the matters required for $LiCoO_2$. The specification of $LiCoO_2$ supplied by a certain company is shown in Table 2.4 as an example. Naturally, the most important property is the electrode density, which is related to the packing density and the density of the sheet electrode. These data are important for the battery manufacturers in order to stuff the cathode active material, such as $LiCoO_2$, into the battery case with constant volume as much as possible. Currently, it seems that 96 wt% of the cathode mixture is $LiCoO_2$ and the residual 4 wt% is the binder and the conductor, such as carbon. Thus, it is important to stuff electroactive $LiCoO_2$ even 1% more. The electrode density within the battery case is increased by the increase in both cathode sheet density and packing density, which leads to the improvement of cell capacity.

Table 2.4 Specification of a $LiCoO_2$ Sample

Item		Impurities	Content (wt%)
Li content (%)	6.60–7.40	Co_3O_4	≤ 1.0
Co content (%)	59.3–60.7	SO_4	≤ 0.30
Li/Co (in mole)	0.95–1.01	H_2O	≤ 0.20
SSA (Specific Surface Area) (m^2/g)	0.35–0.55	Ni	≤ 0.10
D_{50} (average particle size)	7.0–9.0	Cl	≤ 0.10
Aerated density (g/cm^3)	0.9–1.3	Na	≤ 0.050
Packed density (g/cm^3)	1.9–2.3	Fe	≤ 0.020
pH of 10% slurry	9.5–11.0	K	≤ 0.010

It is considered to be important to control the atomic ratio of Li/Co in the production of $LiCoO_2$. One of the features of this product is that its ratio is generally less than one. The cathode slurry is prepared by dispersing the conductor and electroactive $LiCoO_2$ in the N-methyl-pyrrolidone solution containing polyvinylidene fluoride (PVDF). It is unavoidable that some water is contaminated into the slurry. When the unreacted lithium in $LiCoO_2$ remains as Li_2O, it reacts with water in the slurry, and the cathode slurry becomes basic. The cathode slurry changes to a gel state in such basic media; as a result, the cathode slurry cannot be painted onto the aluminum collector. Therefore, conventional raw $LiCoO_2$ is washed with warm water in order to prevent gel formation of the cathode slurry. In an example of the product supplied by a company, the pH of 10 wt% $LiCoO_2$ aqueous dispersion is adjusted to 9.5–11.0. The recommended pH is less than 10.5. This manufacturer supplies $LiCoO_2$ with Li/Co < 1, so there is a possibility for making the unreacted lithium salt in the product close to 0. It can be considered that the washing process of raw $LiCoO_2$ would be removed for cost reduction.

The specific surface area (SSA) also is one of the guidelines, since the reaction area is large when the surface area is large. It is obvious that cathode materials with a high SSA have improved rate performance for high-current discharge. However, the density of the material inevitably decreases when its surface area increases; then the electrode density becomes small. Finally, there is a limitation in enlarging the SSA. Of course, if nanoparticles are used as an electrode-active material, it causes an extreme decrease in density. Further, the battery safety might be seriously ruined even if the rate performance is improved. Therefore, nanosized cathode material could not be recommended. Such materials are not used practically because they have a high possibility of firing in the nail penetration test (a type of battery short-circuit test) and the hot box test (battery heating test in air bath at 150°C).

The desirable average particle size and its distribution are highly related to the coating process of each battery manufacturer. Then, they are different in each battery manufacturer. Moreover, they are different for the type of batteries: prismatic, cylindrical, or polymer batteries, even if they are produced by the same manufacturer. The mass production of the same kind of material is difficult, because these factors are relative to the battery characteristics. The selection of desirable material is also different corresponding to each use or each machine of the battery manufacturer. This is one of the reasons why the manufacturer of cobalt raw material in the world cannot start the mass production of $LiCoO_2$ with the same properties.

The impurities, which cause a redox reaction in the battery, should be removed from product. Remaining Co_3O_4 in the cathode has been viewed with suspicion in recent years. The Co_3O_4 dissolves into the electrolyte as ions during the repetition of discharge. This ion is reduced on the anode and precipitates in the form of metallic Co(0); then the intercalation of Li is obstructed for the increase in the anode impedance. A considerable amount of preliminary information is obtained from the specification of the cathode material as described.

Next, we will explain the synthetic condition of $LiCoO_2$ and its physical and electrochemical characteristics from the viewpoint of actual industrial products. In general, the easiest method to control the physical property of $LiCoO_2$ is to

change its Li/Co ratio. The author already has reported that the structural change from the rhombohedral structure to the monoclinic structure at around 4.1 V disappears by changing the Li/Co atomic ratio to more than 1.[76] In this section, we will explain in detail the physical properties of $LiCoO_2$ with various Li/Co ratio.

SSA decreases with increases in Li/Co, as shown in Fig. 2.16. It is understood that the crystal of $LiCoO_2$ grows easier and sintering of such crystal forms larger particles under the high Li/Co ratio, so it is expected that SSA decreases with increases in the Li/Co ratio. Figure 2.17 shows SEM photographs of $LiCoO_2$ with Li/Co = 1.0 (the left side) and 1.05 (the right side). Although the particle size is about 2–3 μm for the sample with Li/Co = 1.0, the particle size of samples with Li/Co = 1.05 becomes about 10 μm. It is clear that the crystal has grown easily at high Li/Co ratio. The decrease of SSA at high Li/Co ratio also is confirmed as expected.

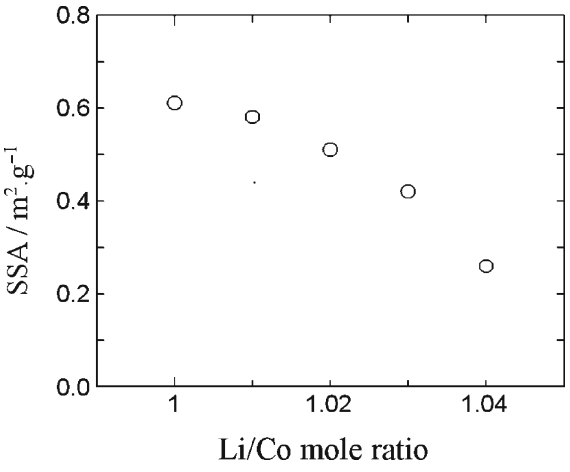

Fig. 2.16 Relation between SSA and Li/Co ratio in $LiCoO_2$

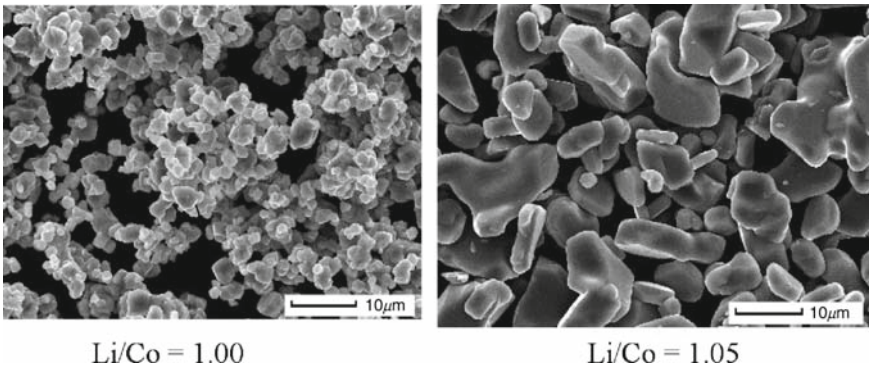

Fig. 2.17 Morphology of $LiCoO_2$ particles with Li/Co mol ratio of 1.00 and 1.05

It would be clear that higher Li/Co ratio is suitable to produce dense material with higher bulk density and higher tap density (Fig. 2.18). Here, it should be noted that the particle size distribution obtained by the wet method is different from that by SEM photograph in some cases. The relations between the Li/Co ratio and the particle size distributions (D_{10}, D_{50}, D_{90}) determined by the microtrack method (wet method) are shown in Fig. 2.19. The particle size of the sample with Li/Co = 1.00 is determined to be as small as 2–3 μm by the SEM photograph; however, the D_{50}, which means average particle size, obtained by the particle size distribution analysis is 10 μm. The differences in particle size by both measurements indicate that the aggregation of the fine particles proceeds under the dispersion in the solution.

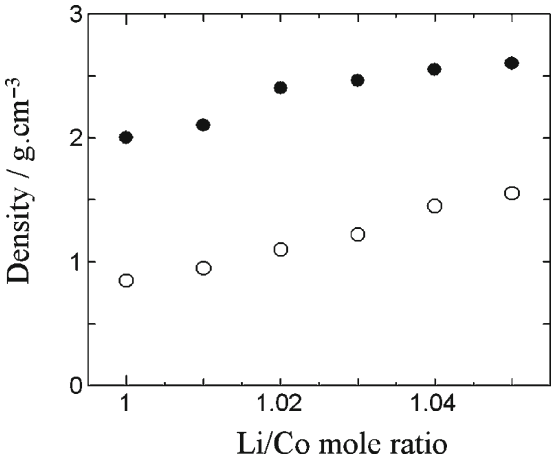

Fig. 2.18 Bulk density (*filled circle*) and tap density (*open circle*) of $LiCoO_2$ with various Li/Co mol ratio

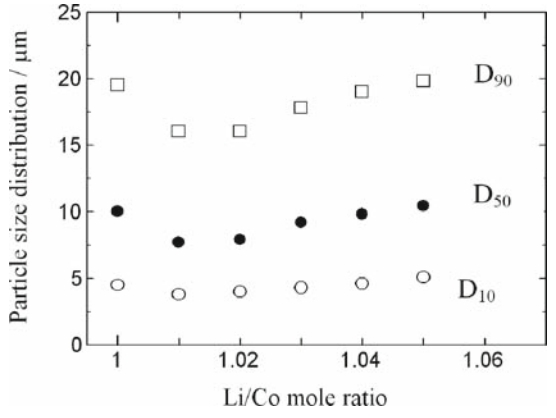

Fig. 2.19 Particle size distribution of $LiCoO_2$ with various Li/Co ratio

In other word, fine particles aggregate in the solution and they are measured as large particles in the case of the wet method. Consequently, measured particle size in the wet method would not reflect the size of primary particles but the size of aggregated secondary particles.

On the other hand, when the particles are growing and become as large as 10 μm in the SEM photograph, the average particle size measured by the microtrack method is D_{50} = 10 μm, as shown in Fig. 2.19. Both methods give the same particle size. The aggregation of particles is protected as the increase in particle size. The particle size distribution reflects the primary particle size in such case. The particle size of the product once decreases and the excess Li remains in product as Li_2O for the synthesis at a higher Li/Co ratio. The amount of remaining Li_2O can be estimated by dispersing $LiCoO_2$ into the aqueous solution and measuring its pH.

The relations between the pH of its 10 wt% suspension and the Li/Co ratio in the raw materials are shown in Fig. 2.20. As the cathode slurry changes to a gel state at the pH > 10.5–10.6, it is necessary to wash the product with warm water for adjusting its pH.

In addition, the effect of the Li/Co ratio on the properties of $LiCoO_2$, such as the crystal size and the pH of the suspension, is described in the paper by the Nippon Chemical Industrial Co., Ltd.[77] Since $LiCoO_2$ with high Li/Co ratio has both a disadvantage and an advantage for the battery characteristics, optimization is required for the synthesis of the product.

Now, let us look back on the history of $LiCoO_2$ synthesis. According to Nishi (Sony Corp.), the synthesis method at the early stage is as follows.[78] The Co_3O_4 and Li_2CO_3 of raw materials are mixed in an aqueous solution containing polyvinyl alcohol to make slurry, and this slurry is baked. In this case, the Li/Co mixing ratio is set at larger than one. The baking temperature is set to be more than 900°C in order to improve the safety of the battery. Moreover, excess Li_2CO_3 remains in the product due to the high Li/Co mixing ratio. However, when this is used as the cathode

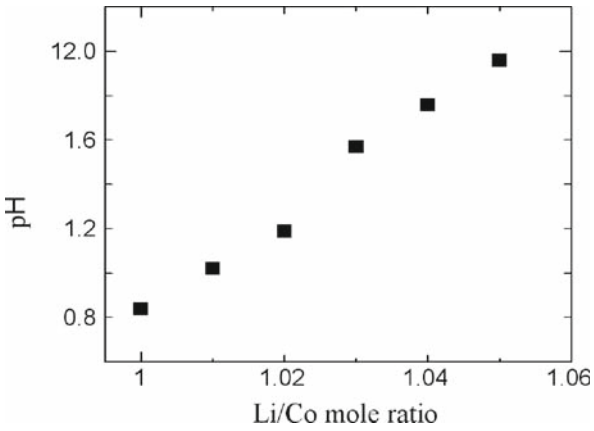

Fig. 2.20 The pH of 10 wt% Li_xCoO_2 slurry

in lithium-ion battery, the remaining Li_2CO_3 generates CO_2 even if the cell is overcharged by any chance. Finally, the battery safety is improved by rupturing the safety valve of the battery by the pressure of generated CO_2 gas. It already has been described that the particle size becomes large and the sintering proceeds more easily at higher Li/Co ratios. It is effective to use the cobalt compound with a large particle size for improving the battery safety, such as the nail penetration test. The $LiCoO_2$ with a large particle size was used in the battery at an early stage. However, the necessity for using such a cathode material with a large particle size has been decreased due to the progress in the battery manufacturing technologies. The recent cathode material has a small particle size as shown in Table 2.4 in order to improve the battery characteristics, especially the high rate performance. Consequently, the highest baking temperature is set lower than 900°C, so that the sintering would not proceed easily. Moreover, it has been found that a part of excess Li_2CO_3 remains in the form of Li_2O after the baking. Recently, the Li/Co ratio is set close to one or slightly lower; thus the remaining Li_2O content after baking has been decreased. In other words, a low-cost process without washing would be used. Such information can be read out from the specification of $LiCoO_2$ supplied by a certain company. The Li/Co ratio decreases very close to 1 and the baking temperature also seems to be decreased. On the other hand, the raw materials, Co_3O_4 and Li_2CO_3, are used now.

However, the production method of $LiCoO_2$ has been changed over the past 2–3 years. Its reason is mainly attributed to the progress in cellular phones. It seems that this new type of $LiCoO_2$ has not been adopted by the battery manufacturer in South Korea and China yet, but it will be used after fiscal year 2003. The pulse discharge mode in the third-generation cellular phone is shown in Fig. 2.21.

In this system, a 2A of maximum current is discharged for 0.6 msec during talking in order to catch the signal for communication. This high current is a considerably excessive requirement for the battery. For instance, much high current, such as a

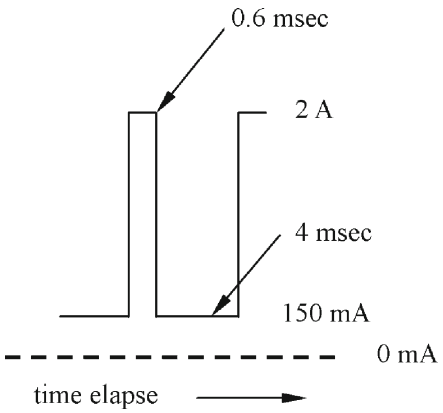

Fig. 2.21 A pulse discharge of GSM-type cellular phone

4-C rate, is discharged for a short time from a battery of 500 mAh/g. Moreover, for the mobile phone, requirements in the cellular phone for high current uses, such as the use of color display, the use of digital camera, and the signal transmission to the satellite capable of an overseas phone call, are steadily increasing. Production methods of $LiCoO_2$ have been improved in order to use the battery at a current of 3-C to 4-C rate. The primary particle size of $LiCoO_2$ is controlled to 1–2 μm for withdrawing such high discharge current. Furthermore, the secondary particle size is controlled to 5–10 μm for keeping a higher density of $LiCoO_2$ and its electrode density. Such increased particle size is also effective in order to avoid the increase in SSA due to the decrease in primary particle size. In order to synthesize this type $LiCoO_2$ with potential of high rate discharge, the synthesis method such as the following hydroxide method has been developed along with the conventional granulation method (solid phase-solid phase method). Currently, the new type of $LiCoO_2$ has been synthesized mainly by the hydroxide method. The raw material would be changed from the conventional cobalt oxide to the cobalt hydroxide. In this method, the precipitate of the hydroxide is synthesized by increasing the pH of aqueous cobalt solution to more than 7. In this case, the precipitation condition, the pH, the aging temperature, and so forth are controlled to get particles with desirable size and shape. Afterward, the precipitate is mixed with the Li_2CO_3 and baked to synthesize $LiCoO_2$. Now, let us introduce an example with a spherical shape in particular. Its SEM image is shown in Fig. 2.22. It can be seen that the primary particles with 1–2 μm aggregate and form the secondary particles with ca. 10 μm. This homogeneous spherical size type of $LiCoO_2$ cannot be used as a cathode of lithium-ion batteries, because the packing density is not enough. A battery using the $LiCoO_2$ with loosely formed secondary particles is shown in Fig. 2.22 (left).

An active material whose physical properties and chemical properties fit the requirements, such as the standard of the targeted battery, the specification of the electrode based on the battery, and the balance with the submaterials except for an electroactive material is selected. The accumulation of data, which can fulfill any requirement, would be important.

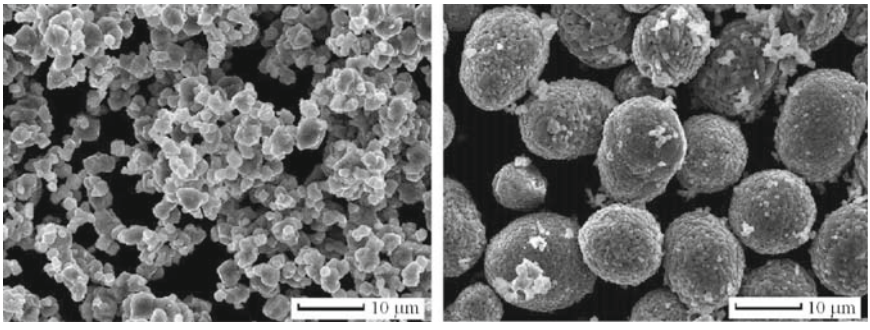

Fig. 2.22 SEM photograph of $LiCoO_2$ with different types of secondary particles

2.5.2 Recent Layered Nickel-Based Cathode Materials

In the $LiNiO_2$ type materials, the chemical formula of the prepared sample would be basically described as $Li_{1-x}Ni_{1+x}O_2$ ($x > 0$). A strict preparation condition is required because a part of the nickel ions may occupy the lithium-ion layer. Therefore, the following three synthesis methods, by which the raw materials can be mixed in the atomic level, are usually applied (the solid-state method is basically not suitable to prepare pure material):

- Spray drying method
- Hydroxide method
- Mixed metal carbonate method

All these methods are a kind of co-precipitation method. It is possible to mix several elements at the atomic level by using such a co-precipitation technique. These methods have the advantages in the control of the primary particle size and the secondary particle size against the solid-state method, that is, the fine particle control becomes possible. Furthermore, it has the advantage of enabling the control of crystallinity and the surface morphology. However, in some cases, this method might not be practically used for mass-production because the processing technology is too elaborate.

The sol-gel method is frequently reported as a synthesis method in the laboratory. However, the description about this method is omitted because production cost is too expensive and this method is not suitable for industrial mass production except for an experimental use.

2.5.2.1 Synthesis by Spray-Drying Method

The spray-drying method,[79] developed by Toda Kogyo Co. (formerly Fuji Chemical Industry Co.) is well known. Their sample was shipped to many companies worldwide, and it has been confirmed that it has excellent characteristics. In particular, the safety test has been finished in Saft Co. in France and in Samsung in South Korea in 1999. Those results were disclosed to the public at the international congress. According to what I heard, Saft Co. selects the nickel-based material as the cathode material of the lithium-ion battery for EV, concluding that the capacity fading problem of the manganese-based cathode at elevated temperatures would not be overcome. Moreover, this material has been practically used as the battery material mainly in foreign corporations up to now. According to these patents, metal salt and lithium salt are reacted in an aqueous medium and the obtained slurry is baked at the desirable temperature after spray drying.

In the product of Toda Kogyo Co., aluminum doping is its feature. The features of this product are that the shortcoming of the thermal instability, which is a fault of the nickel-based cathode material, has been overcome by cobalt and aluminum doping. The thermal stability at the charged state has been improved to the $LiCoO_2$ level in particular. The composition of the compound shipped is announced to be

$Li_{0.8}Co_{0.15}Al_{0.05}O_2$. The data about the thermal stability of this compound obtained by Binsan et al. of Saft Co.[80] are shown in Table 2.5.

It can be understood that the temperature of the exothermic peak with oxygen evolution increased from 200°C of $LiNiO_2$ to 310°C of $LiNi_{0.8}Co_{0.15}Al_{0.05}O_2$ due to the decrease in the nickel content and the aluminum doping. The thermal stability of this compound has been considerably improved. The oxygen evolution was not observed below 300°C. On the whole, the thermal stability of this is more excellent than that of $LiCoO_2$ and comparable to that of spinel $LiMn_2O_4$. In addition, the SEM image of this material is shown in Fig. 2.23. It would be possible to control the powder characteristics the same as the co-precipitation method. It is clear from Table 2.5 that this material has a larger capacity than that of the cobalt-based cathode. This cathode delivers more than 180 mAh/g for 4.3 V charge, as shown in Fig. 2.24.

Recently, an example of the laminate-type battery combined this material and the high-capacity graphite was reported from Toshiba Battery Co.[81] The prismatic battery (thickness: 3.8 mm and area: 35 × 62 mm) exhibits a capacity of 920 mAh and its energy density is 200 Wh/g, which is 16% larger than that of the cobalt-based cathode. These data seem to largely contribute to the practical use of the nickel-based battery. The rate performance of this battery is also excellent, as shown in Fig. 2.25. The charge/discharge capacity after 500 cycles of charge/discharge test in 1-C rate keeps 70% of the initial capacity, which is comparable to the cobalt cathode-based batteries.

Table 2.5 Thermal stability of typical cathode materials and $LiNi_{0.8}Co_{0.15}Al_{0.05}O_2$ in charged state

Cathode materials	$LiNiO_2$	$LiCoO_2$	$LiMn_2O_4$	$LiNi_{0.8}Co_{0.15}Al_{0.05}O_2$
Initial charge capacity (mAh/g, 4.2 V)	210	160	130 (4.3 V)	205
Reversible capacity (mAh/g)	165	150	120	160
Temperature of highest heat flow in DSC main peak under the existence of solvent	200	250	300	310
Oxygen evolution temp. from charged cathode material (4.2 V)	200	230	290	300

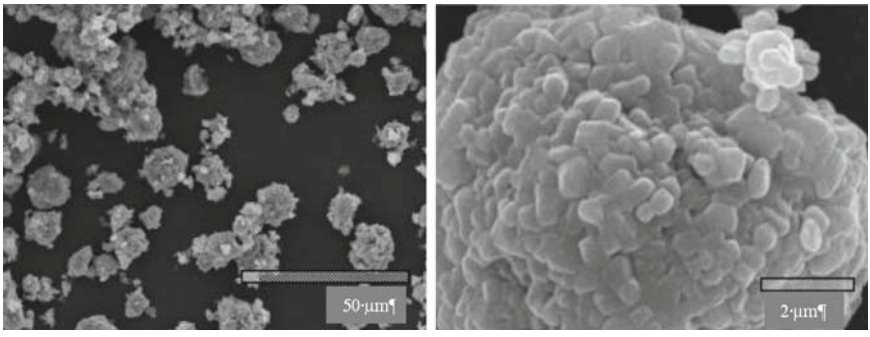

Fig. 2.23 SEM images of morphology controlled $LiNi_{0.8}Co_{0.15}Al_{0.05}O_2$

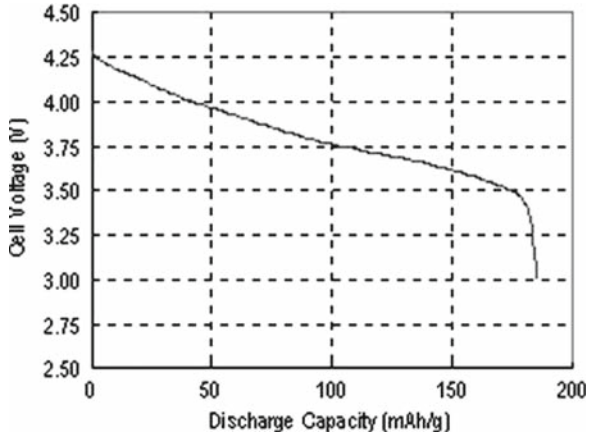

Fig. 2.24 Discharge curve of $LiNi_{0.8}Co_{0.15}Al_{0.05}O_{2.}$

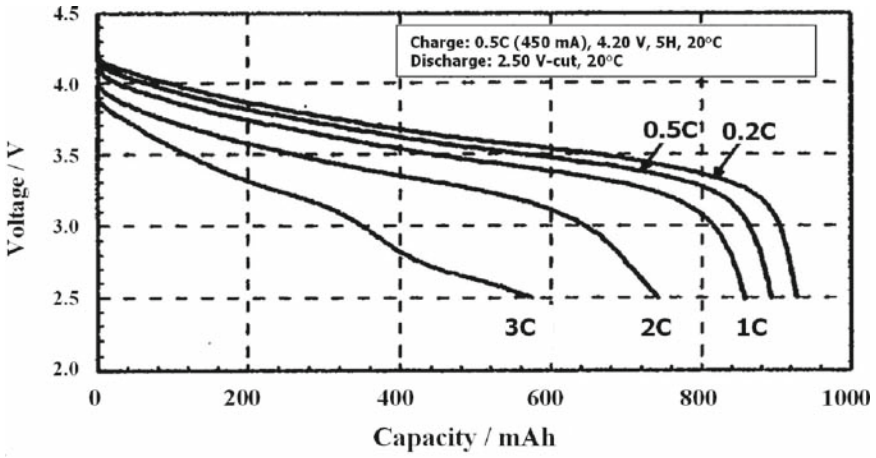

Fig. 2.25 Rate performance of laminate-type lithium ion battery composed of $LiNi_{0.8}Co_{0.15}Al_{0.05}O_2$ cathode and graphite anode

2.5.2.2 Synthesis by the Hydroxide Method

The procedure developed by Tanaka Chemical Co. is in the forefront of these methods. This company occupies almost a monopoly position as a supplier of cathode materials for the nickel–cadmium battery and the nickel–metal hydride battery. Metal hydroxides have been prepared via an amine complex. Spherical material is produced by adjusting the pH of the aqueous solution, the aging temperature, and the introduction rate of the reactant. This technology is applied to the cathode material of lithium-ion batteries and has been patented.[82] Since precipitates with homogeneous distribution of various elements can be obtained using the co-precipitation technique,

this method can be considered to be an excellent method. The cobalt hydroxide prepared by the particle shape control technique was developed by Tanaka Chemical Co. Various kinds of particles with different morphorogies, such as the aggregated fine particles, the aggregated plate-like crystals, the aggregated large-size particles, and the isolated large-size particles, can be obtained by controlling the co-precipitation condition. The cathode material for the lithium-ion battery is synthesized by baking after mixing the lithium salt with the raw hydroxide. In this case, it also is important to maintain the particle shapes of raw materials by controlling the heating condition. Fundamentally these types of hydroxides were supplied by Tanaka Chemical Co. and were synthesized to cathode material.

Ohzuku[83] and Dahn in Canada have synthesized $LiNi_{0.5}Mn_{0.5}O_2$ and $LiNi_{1/3}Mn_{1/3}Co_{1/3}O_2$, using the nickel/manganese co-precipitate and the nickel/manganese/cobalt co-precipitate, which are precursors developed in this company. Such cathode materials attract much attention because of the large battery capacity. Here, the data obtained by Ohzuku are shown in Fig. 2.26.[83] Both of them have a capacity of about 200 mAh/g, and they would be promising materials in the future. However, they have a disadvantage in the high-rate performance; improvements in rate capability are being advanced at present. In addition, the nickel/manganese/cobalt co-precipitate with higher tap density, as 2.0–2.3 g/cm^3, is supplied.

2.5.2.3 Mixed Metal Carbonate Method

The hydroxide co-precipitation method is an excellent method as previously described. However, the process for hydroxide co-precipitate containing manganese ion would be difficult in the processing technology. Since hydroxide

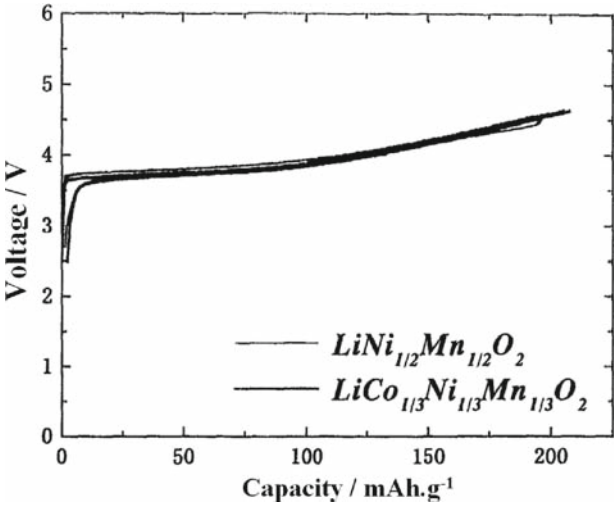

Fig. 2.26 Charge/discharge curves of $LiNi_{1/2}Mn_{1/2}O_2$ and $LiCo_{1/3}Ni_{1/3}Mn_{1/3}O_2$

co-precipitation is carried out in basic conditions, the manganese ion can stay as 2^+, 3^+, or 4^+ ion. As oxygen in air promotes the oxidation of manganese ion, therefore, it seems considerably difficult to synthesize the identical co-precipitate reproducibly. It can be assumed from their patent that at Tanaka Chemical Co. the manganese ion is co-precipitated from the Mn^{2+}-amine complex as $Mn(OH)_2$ under a reducing agent for overcoming this difficulty.

On the other hand, the so-called mixed metal carbonate method developed by Chuo Denki Kogyo Co.[84,85] is a kind of co-precipitation method, where metal salt is co-precipitated as a carbonate or bicarbonate under the presence of bicarbonate in basic solution. This method seems to be an excellent method without the shortcoming of the hydroxide co-precipitation method as mentioned above. As this method also is a kind of co-precipitation method, the control of particle shape is naturally possible and the spherical particles with high density also are obtained. The initial capacity of $LiNi_{0.56}Mn_xCo_{0.44-x}O_2$ synthesized by this method and the peak temperature measured by DSC in coexistence with the electrolyte are shown in Table 2.6. It is obvious that the DSC peak temperature related to the oxygen evolution shifts

Table 2.6 Electrochemical properties and thermal properties of $LiNi_{0.56}Mn_xCo_{0.44-x}O_2$ (x = 0.1, 0.2, and 0.3)

Compounds	Initial capacity (mAh/g)	Average voltage (V)	Peak temp. in DSC (°C)	Heat generation (J/g)
$LiNi_{0.56}Mn_{0.1}Co_{0.34}O_2$	173	3.78	298	728
$LiNi_{0.56}Mn_{0.2}Co_{0.24}O_2$	171	3.81	300	645
$LiNi_{0.56}Mn_{0.3}Co_{0.14}O_2$	167	3.84	316	577
$LiNiO_2$	183	3.84	225	1,398
$LiCoO_2$	156	3.97	251	616

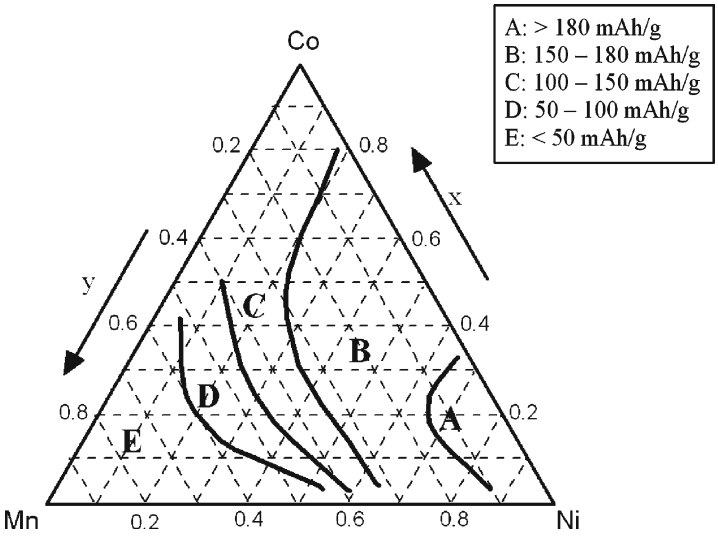

Fig. 2.27 Discharge capacity of $LiNi_{1-x-y}Co_xMn_yO_2$

to the higher temperature as the increase in manganese doping amount and the amount of heat generation decreases extremely. Namely, the safety of the battery is improved by manganese doping. Moreover, its initial capacity is higher than that of $LiCoO_2$. Its energy density (product of capacity and voltage) is higher still because of its higher discharge voltage.

The battery manufacturers using this compound as the cathode-active material prepare large-size batteries with 100 Wh class or 400 Wh class. Their cycle life, thermal behavior, high-rate performance, effect of storage at charged state on the electrochemical property, and so forth have been estimated. The battery shows a capacity retention of 83% after 1,000 cycles. Furthermore, it has been proved that the thermal stability is increased as the manganese content increases, that the manganese content should not exceed 0.35 because of the extreme expansion of the *c*-axis, and that the manganese or cobalt content in it does not have an impact on the charge/discharge curve. Figure 2.27 shows the ternary phase diagram by Terasaki et al., which indicates the relations between capacity and composition of $LiNi_{1-x-y}Co_xMn_yO_2$. They have reported that samples are prepared from mixed metal carbonate. Probably, the mixed metal carbonate precursor would make it possible to prepare $LiNi_{1-x-y}Co_xMn_yO_2$, the wide composition range.

References

1. M. Zou, M. Yoshio, S. Gopukumar, J. Yamaki, *Electrochem. Solid-State Lett.*, **7** (2004) A176
2. W.S. Yoon, Y. Paik, X.Q. Yang, M. Balasubramanian, J. McBreen, C.P. Grey, *Electrochem. Solid-State Lett.*, **5** (2002) A263
3. A.R. Armstrong, P.G. Bruce, *Nature*, **381** (1996) 499
4. G. Vitins, K. West, *J. Electrochem. Soc.*, **144** (1997) 2587
5. M. Tabuchi, K. Ado, H. Kobayashi, H. Kageyama, C. Masquelier, A. Kondo, R. Kanno, *J. Electrochem. Soc.*, **145** (1998) L145
6. Y.I. Jang, B. Huang, H. Wang, D.R. Sadoway, Y.M. Chiang, *J. Electrochem. Soc.*, **146** (1999) 3217
7. Y.S. Lee, M. Yoshio, *Electrochem. Solid-State Lett.*, **4** (2001) A166
8. Y.S. Lee, Y.K. Son, M. Yoshio, *Chem. Lett.*, **30** (2001) 882
9. J.M. Paulsen, C.L. Thomas, J.R. Dahn, *J. Electrochem. Soc*., **147** (2000) 861
10. J.M. Paulsen, J.R. Dahn, *J. Electrochem. Soc.*, **147** (2000) 2478
11. J.M. Paulsen, D. Larcher, J.R. Dahn, *J. Electrochem. Soc.*, **147** (2000) 2862
12. T. Ohzuku, A. Ueda, M. Nagayama, *J. Electrochem. Soc.*, **140** (1993) 1862
13. W. Li, J.N. Reimers, J.R. Dahn, *Solid State Ionics*, **67** (1993) 123
14. H. Arai, S. Okada, H. Ohtsuka, M. Ichimura, J. Yamaki, *Solid State Ionics*, **80** (1995) 261
15. J.N. Reimers, J.R. Dahn, *J. Electrochem. Soc.*, **139** (1992) 2091
16. T. Ohzuku, A. Ueda, *J. Electrochem. Soc.*, **141** (1994) 2972
17. G.G. Amatucci, J.M. Tarascon, L.C. Klein, *J. Electrochem. Soc.*, **143** (1996) 1114
18. S. Levasseur, M. Menetrier, E. Suard, C. Delmas, *Solid State Ionics*, **128** (2000) 11
19. M. Yoshio, H. Noguchi, K. Yamato, J. Itoh, M. Okada, T. Mouri, *J. Power Sources*, **74** (1998) 46
20. A. Von der Ven, M.K. Aydinol, G. Ceder, *J. Electrochem. Soc*., **145** (1998) 2149
21. J.M. Paulsen, J.R. Mueller-Neuhaus, J.R. Dahn, *J. Electrochem. Soc.*, **147** (2000) 508
22. D. Carlier, I. Saadoune, M. Menetrier, C. Delmas, *J. Electrochem. Soc.*, **149** (2002) A1310

23. X.Q. Yang, J. McBreen, W.S. Yoon, C.P. Gray, *Electrochemistry Comm.*, **4** (2002) 649
24. D. Li, T. Muta, L. Zhang, M. Yoshio, H. Noguchi, *J. Power Sources*, **132** (1998) 150
25. J.M. Paulsen, C.L. Thomas, J.R. Dahn, *J. Electrochemcal Soc.*, **146** (1999) 3560
26. J.M. Tarascon, D. Guyomard, *J. Electrochem. Soc.*, **138** (1991) 1378
27. R.J. Gummor, D.C. Likes, M.M. Thackeray, *Mat. Res. Bull.*, **28** (1993) 1249
28. G. Vitins, K. West, *J. Electrochem. Soc.*, **137** (1990) 769
29. J.M. Paulsen, J.R. Dhan, *J. Electrochem. Soc.*, **147** (2000) 2478.
30. M. Yoshio, H. Nakamura, Y. Xia, *Electrochim. Acta*, **45** (1999) 273
31. P. Dan, E. Mengeritsky, D. Aurbach, I. Weissman, E. Zinigrad, *J. Power Sources*, **68** (1997) 443
32. E. Levi, E. Zinigrad, H. Teller, M.D. Levi, D. Aurbach, *J. Electrochem. Soc.*, **145** (1998) 3440
33. Y.S. Lee, N. Kumada, M. Yoshio, *J. Power Sources*, **96** (2001) 376
34. N. Imachi, I. Nakane, K. Narukawa, *Sanyo Technical Review*, No.**34** (2004)79
35. S. Yoshimura, *Technical Report (Sanyo),* **2** (2004) 119
36. Y. Xia, M. Yoshio, *J. Power Sources*, **66** (1997) 129
37. T. Nohma, H. Kitao, Manuscript in *Battery Technology Committee* (Japan), 16–3 (2004)
38. S. Komaba, N. Kumagai, Y. Kataoka, *Electrochim. Acta*, **47** (2002) 1229
39. Y. Yagi, Y. Hideshima, M. Sugita, H. Noguchi, M. Yoshio, *Electrochemistry*, **68** (2000) 252
40. X. Yang, X. Sun, M. Balasubramanian, J. McBreen, Y. Xia, T. Sakai, M. Yoshio, Electrochem. *Solid State Lett.*, **4**, (2001) A117
41. Y. Xia, M. Yoshio, *J. Electrochem. Soc.*, **144** (1997) 4186
42. D.J. Jang, Y.J. Shin, S.M. Oh, *J. Electrochem. Soc.*, **143** (1996) 2204
43. H. Yamane, M. Saitoh, M. Sano, M. Fujita, M. Sakata, M. Takada, N. Nishibori, *J. Electrochem. Soc.*, **149** (2002) A1514
44. M. Zou, M. Yoshio, S. Gopukumar, J. Yamaki, *Mat. Res. Bull.*, **40** (2005) 708
45. K. Oikawa, T. Kamiyama, F. Izumi, B.C. Chakoumakos, H. Ikuta, M. Wakihara, J. Li, Y. Matsui, *Solid State Ionics*, **109** (1998) 35
46. B. Deng, H. Nakamura, Q. Zhang, M. Yoshio, Y. Xia, *Electrochim. Acta*, **49** (2004) 1823
47. H. Noguchi, H. Nakamura, M. Yoshio, H. Wang, *Chem. Lett.*, **33** (2004) 546
48. M. Yoshio, H. Noguchi, Y. Todorov and Y. Hideshima, *Denki Kagaku*, **66** (1998) 189
49. G.T.K. Fey, W. Li, J.R. Dahn, *J. Electrochem. Soc.*, **141** (1994) 227
50. G.T.K. Fey, C.S. Wu, *Pure Appl. Chem.*, **69** (1997) 2329
51. Y. Xia, M. Yoshio, *J. Electrochem. Soc.*, **143** (1996) 825
52. Y. Xia, Y. Zhou, M. Yoshio, *J. Electrochem. Soc.*, **144** (1997) 2593
53. M. Yoshio, J. Taira, H. Noguchi, K. Isono, *Electrochemistry*, **66** (1998) 335
54. Y.M. Todorov, Y. Hideshima, H. Noguchi, M. Yoshio, *J. Power Sources*, **77** (1999) 198
55. Y. Terada, K. Yasaka, F. Nishikawa, T. Konishi, M. Yoshio I. Nakai, *J. Solid State Chem.*, **156** (2001) 286
56. H. Kawai, M. Nagata, H. Tsukamoto, A.R. West, *J. Power Sources*, **81–82** (1999) 67
57. T. Ohzuku, K. Ariyoshi, S. Yamamoto, *J. Ceram. Soc. Jpn.*, **110** (2002) 501
58. S.-H. Park, Y.-K. Sun, *Electrochim. Acta*, **50** (2004) 434
59. S. Mukerjee, X.Q. Yang, X. Sun, S.J. Lee, J. McBreen, Y. Ein-Eli, *Electrochim. Acta*, **49** (2004) 3373
60. A.K. Padhi, K.S. Nanjundaswamy, J.B. Goodenough, *J. Electrochem. Soc.*, **144**, (1997) 1188
61. A.S. Andersson, J.O. Thomas, *J. Power Sources*, **97–98** (2001) 498
62. M. Takahashi, S. Tobishima, K. Takei, Y. Sakurai, *J. Power Sources*, **97–98** (2001) 508
63. J.R. Dahn, E.W. Fuller, M. Obrovac, U. von Sachen, *Solid State Ionics*, **69** (1994) 265
64. H. Arai, S. Okada, Y. Sakurai, J. Yamaki, *Solid State Ionics*, **109** (1998) 295
65. K.K. Lee, W.S. Yoon, K.B. Kim, K.Y. Lee, S.T. Hong, *J. Power Sources*, **97–98** (2001) 321
66. M.G.S.R. Thomas, W.I.F. David, J.B. Goodenough, *Mat. Res. Bull.*, **15** (1980) 783
67. R. Kanno, H. Kubo, Y. Kawamoto, T. kamiyama, F. Izumi, Y. Takeda, M. Takano, *J. Solid State Chem.*, **110** (1994) 216
68. D.D. MacNeil, Z. Lu, Z. Chen, J.R. Dahn, *J. Power Sources*, **108** (2002) 8
69. Y. Gao, M.V. Yakovleva, W.B. Ebner, *Electrochem. Solid State Lett.*, **1** (1998) 117

70. J. Cho, H.S. Jung, Y.C. Park, G.B. Kim, H.S. Lim, *J. Electrochem. Soc.*, **147** (2000) 15
71. T. Ohzuku, T. Yanagawa, M. Kouguchi, A. Ueda, *J. Power Sources*, **68** (1997) 131
72. J. Cho, B. Park, *J. Power Sources*, **92** (2001) 35
73. Japan Patent, H11-307094, 2001-128249
74. M. Zou, M. Yoshio, S. Gopukumar, J. Yamaki, *Chem. Mater.*, **15** (2003) 4699
75. M. Zou, M. Yoshio, S. Gopukumar, J. Yamaki, *Chem. Mater.*, **17** (2005) 1284
76. S. Tobishima, K. Takei, Y. Sakurai, J. Yamaki, *J. Power Sources*, **90** (2000) 188
77. K. Ikeda, *Lithium Ion Secondary Battery*, 2nd ed. M. Yoshio and A. Kozawa(editors), p.292, 2000, Nikkan Kogyou Shinbunsha, Tokyo
78. N. Yomasaki, Recent battery technology, *Semin.Electrochem.,* **1**, (1977) 77, Electrochemical Society of Japan
79. M. Nishi, *Topics on Lithium Ion Secondary Battery*, Shokabou, (1977)
80. Patent No. WO/06679, Kokai Tokkyo Kouhou H10-069910
81. Ph. Binsan, *J. Power Sources*, **81–82** (2003) 906
82. N. Takami et al., 11th IMLB, Ab. No. **371** (2002)
83. Japan patent, 2002–201028, H9-270256
84. T. Ohzuku, K. Ariyoshi, S. Yamamoto, Y. Makimura, *Chem. Lett.*, **30** (2001) 1270
85. K. Yamato, K. Kobayashi, S. Ota, K. Hayashi, K. Kitamura, T. Miyashita, 41th Battery Symposium, p.386 (2000)